Tampere University of Technology

Department of Information Technology

Kim Östman

A Gigahertz-range High-*Q* VCO

Master of Science Thesis

The subject of this thesis was approved by the Council of the Department of Information Technology on April 6, 2005.

Examiners: Professor Nikolay Tchamov, TUT

Dr. Ivan Uzunov, Senior Researcher, TUT

Acknowledgments

There are many people who deserve thanks for getting me to this point in my studies. I cannot name them all, but in any case I'd like to give specific credit to a few of them.

First of all I'd like to thank Professor Nikolay Tchamov for providing a secure environment in which to perform the work that this thesis is based on. The funding was mostly provided by the European Union through the 5th framework research project MARTINA (IST-2001-37362). Professor Tchamov's and Dr. Ivan Uzunov's comments and suggestions in performing this work are much appreciated. I'd also like to thank all of my colleagues for making the work environment in the research group Analog Circuits for Digital Communications very friendly and encouraging. Especially I would like to thank Hristo Brachkov, Svetozar Broussev, and Sami Sipilä for their efforts to mentor me in the art of RF IC design.

I would also like to thank my parents Bertel and Ruusa and my sister Anne-Maria together with her family for their continued support. Most of all I would like to thank my parents for providing me a good home and upbringing during my basic schooling and for encouraging me to study as far as I can when I left home for the big wide world.

Tampere on November 15, 2005

Kim Östman
Ruovedenkatu 20 E 76
33720 Tampere
Tel: +358 – 40 – 829 6192

Table of Contents

List of Figures

List of Tables

Tampere University of Technology
Department of Information Technology
Institute of Communications Engineering

Kim Östman: A Gigahertz-range High-*Q* VCO
Master of Science Thesis: xii + 64 pages, 26 pages in appendices, December 2005

Examiners: Professor Nikolay Tchamov
Dr. Ivan Uzunov, Senior Researcher

Keywords: VCO, FBAR
Funding: The European Union under project IST-2001-37362
(MARTINA)

Abstract

This thesis presents the theory, design, and measurements of two fully monolithic voltage-tunable above-IC-FBAR oscillators for 2.1 GHz in 0.25-µm SiGe BiCMOS technology. The narrow-band FBAR devices were built above the SiGe circuits during post-processing steps. The oscillators are based on a two-transistor loop structure and use the above-IC FBAR in its series-resonant mode. One of the oscillators has a single-ended output, and the other one is implemented with a differential output.

The oscillators show a significant improvement in phase noise performance compared to a reference LC VCO fabricated in the same process, with the best phase noise being -144.1 dBc/Hz at an offset of 1 MHz and -149.6 dBc/Hz at 3 MHz. The architecture offers advantages in overcoming frequency tuning difficulties usually present when using high-*Q* resonators. Although the used frequency tuning solution compromises phase noise performance, the measured tuning range of 37 MHz is the highest yet reported for FBAR oscillators.

Tampereen teknillinen yliopisto
Tietotekniikan osasto
Tietoliikennetekniikan laitos

Kim Östman: A Gigahertz-range High-*Q* VCO
Diplomityö: xii + 64 sivua, 26 liitesivua, Joulukuu 2005

Tarkastajat: Professori Nikolay Tchamov
Tri Ivan Uzunov, vanhempi tutkija

Avainsanat: VCO, FBAR
Rahoitus: Euroopan Unioni projektin IST-2001-37362 (MARTINA) puitteissa

Tiivistelmä

Tässä diplomityössä esitetään kahden täysin monoliittisen jänniteohjatun oskillaattorin teoria, suunnittelu ja mittaukset. Piirit on toteutettu 2.1 GHz:n taajuusalueelle 0.25-µm SiGe BiCMOS puolijohdeteknologialla ja niissä käytetään mikrosirun päälle kasvatettua FBAR-resonaattoria. Nämä kapeakaistaiset resonaattorit kasvatettiin SiGe-piirien päälle varsinaisen puolijohdeprosessin jälkeen. Oskillaattorit perustuvat kahden transistorin silmukkarakenteeseen ja käyttävät sirun yläpuolella olevaa resonaattoria sarjaresonanssitilassa. Ulostulo on piiristä riippuen toteutettu epäsymmetrisenä tai differentiaalisena.

Näiden kahden oskillaattorin vaihekohina on huomattavasti parempi kuin vertailua varten samassa prosessissa valmistetulla LC-oskillaattorilla. Paras vaihekohina on -144.1 dBc/Hz yhden megahertsin etäisyydellä kantoaallosta ja -149.6 dBc/Hz kolmen megahertsin etäisyydellä. Oskillaattoriarkkitehtuuri tuo mukanaan etuja, joiden avulla korkean hyvyysarvon resonaattorien yleensä mukanaan tuomat taajuudensäätövaikeudet pienenevät. Vaikka käytetty säätömenetelmä heikentääkin vaihekohina-arvoja, on mitattu 37 MHz:n säätöväli suurin FBAR-oskillaattoreilla tähän mennessä saavutettu.

Abbreviations

AC	Alternating Current
BAW	Bulk Acoustic Wave
BiCMOS	Bipolar Complementary Metal Oxide Semiconductor
CEA-LETI	Commissariat á l'Énergie Atomique – Laboratoire d'Electronique de Technologie de l'Information
CSEM	Centre Suisse d'Electronique et de Microtechnique SA
DC	Direct Current
DCO	Digitally Controlled Oscillator
DRC	Design Rules Check
FBAR	Film Bulk Acoustic Resonator
FOM	Figure of Merit
GSM	Global System for Mobile Communications
IC	Integrated Circuit
ICO	Current Controlled Oscillator
LED	Light-Emitting Diode
LVS	Layout Versus Schematic
MBVD	Modified Butterworth-Van Dyke
MIM	Metal Insulator Metal
PCB	Printed Circuit Board
RF	Radio Frequency
SAW	Surface Acoustic Wave
SiGe	Silicon Germanium

THD	Total Harmonic Distortion
VCO	Voltage Controlled Oscillator
VCSO	Voltage Controlled SAW Oscillator
WCDMA	Wideband Code Division Multiple Access
XO	Crystal Oscillator

Symbols

f	Frequency
C	Capacitance
g_m	Transconductance
I	Current
L	Inductance
P	Power
Q	Quality factor
Q_i	Bipolar transistor
R	Resistance
V_{CC}	Supply voltage
V_{CTRL}	Control voltage

Introduction

Oscillators are circuits that produce a periodic AC signal at a desired frequency. These circuits have a very important role in modern-day communication equipment, and they are used in all devices that employ either a transmitter or a receiver, or both (a transceiver). Oscillators are usually utilized in receivers and transmitters in connection with a mixer when a radio signal needs to be up-converted or down-converted in frequency.

Some oscillators operate on only one frequency, and therefore they do not necessarily need to be controlled in any way. However, great benefits are obtained by making an oscillator controllable, meaning that it can cover a range of frequencies instead of just one fixed frequency. This enables the radio device that uses the oscillator to operate on many different frequencies.

Oscillator behavior can be quantified by certain parameters, including power consumption and frequency range. Portable communication devices such as mobile phones usually use a limited source of energy, and it is therefore important to not drain this source of energy too quickly. The power consumption of the device, including the oscillator, should therefore be as small as possible. The frequency range of the oscillator determines the usable frequency range of the complete communication device, and it should therefore be as large as possible, or at least large enough to cover the desired communication band.

An especially important parameter for describing oscillator performance is the phase noise of the oscillator. Phase noise is a way of quantifying frequency stability. In modern-day communication standards, it is very important that radio devices stay within

their allotted frequency ranges and cause no disturbance to other users who are receiving signals on adjacent frequencies. The devices should therefore have superior frequency stability. This makes oscillator phase noise a critical issue, because the frequency stability of the oscillator determines the frequency stability of the complete radio transceiver. For some communication standards, such as GSM, the stability specifications are very strict.

Many features in the electrical circuits of oscillators are known to have an adverse effect on frequency stability. Depending on the oscillator circuit topology, the most critical factors can include transistor sizing and the quality factors of some reactive components. Making a transistor too small can cause excessive electronic noise in the circuit, which in turn is converted into frequency instability. Reactive components such as inductors and capacitors are employed by a special type of oscillators generally called harmonic oscillators or LC oscillators. The overall oscillator circuit usually operates on or close to the resonance frequency of the LC resonator. The quality factor of the resonator is perhaps the most critical feature influencing phase noise performance in these LC oscillators, thus forcing the designer to seek to employ a resonator with as high a quality factor as possible.

Components with low quality factors have been a constant concern among designers who are trying to develop high-performance oscillators. LC resonator quality factors have generally been very low in integrated circuits, with the maximum presently being around 20. Inductors and capacitors in integrated circuits have substantially lower quality factors than their discrete counterparts, the low quality factor being a result of the way electronic components are integrated on silicon microchips. The low quality factor means that the components include large loss resistances and thus generate electronic noise. These components also cause greater energy losses in circuits, resulting in increased power consumption. On the one hand, it is easier to design oscillators with broad frequency ranges when using these low-quality-factor components. On the other hand, however, this benefit is severely at odds with the decreased phase noise performance, often the most important issue when designing reliable and stable oscillators for radio devices.

Crystals and various surface-acoustic wave (SAW) and bulk-acoustic wave (BAW) devices may be used when implementing resonators in oscillators, and they enable very good phase noise performance. The film bulk acoustic resonator (FBAR) is one relatively recent development in the family of BAW devices. The problem with the FBAR (and BAW devices in general) is that it is costly and not automatically compatible with IC

processes, and due to its mechanical construction the frequency tunability of FBAR oscillators becomes very difficult.

Recent research has sought to utilize FBAR devices by building them above silicon chips. The FBAR may in these cases save chip real estate by replacing monolithic inductors and/or LC tanks. This approach has been combined with radio-frequency (RF) integrated circuit design and used for example in a filtering low-noise amplifier [1], [2], and an experimental RF front-end [3] to realize a bandpass filter, with the above-IC FBARs replacing the traditional off-chip components. It has also been used to implement stand-alone filters [4]. Although general problems related to extra processing step costs, yield, and tolerances remain, it has become clear that FBAR technology can be successfully combined with standard IC processes. One major obstacle to making integrated high-*Q* VCO circuits is thus overcome.

The purpose of this study is to present the design of two near-identical oscillators, both utilizing an above-IC FBAR resonator that has a quality factor considerably higher than traditional LC resonators. An additional LC oscillator is designed for reference purposes. In theory, making the change should have a noticeable effect on the phase noise performance and the frequency tuning range of the oscillator. The study will confirm this theory by presenting the measurement results of the LC oscillator and two versions of the FBAR oscillator. In spite of the problem of a decreased frequency range in the FBAR oscillator, it has improved phase noise performance and is shown to be a viable alternative in future wireless communications applications.

The contents of this thesis are organized as follows. Chapter one deals with general oscillator theory, explaining different oscillator types and parameters. The second chapter contains a brief literature review and takes a look at the issues involved in using an FBAR in oscillators. Chapter three describes the oscillator architecture used in the present work, with chapters four and five presenting LC and FBAR based implementations of the oscillator, respectively. The sixth chapter compares these two implementations by highlighting the pros and cons of both approaches. The final chapter presents conclusions derived from the work encompassed by this thesis and suggests directions for further research involving integrated high-*Q* VCO circuits.

1 Oscillator Theory

An oscillator is a circuit that consumes DC power and produces a repetitive or periodic AC signal at its output. No input signals except for the power supply are needed for the oscillations to occur. This theoretical chapter provides a brief look into two main ways of making oscillators, discusses the criteria that must be fulfilled for a circuit to produce oscillations, describes how an oscillator's output frequency can be controlled, reviews the effects of resonator quality factor on different facets of oscillator performance, and finally lists some of the most important performance metrics used to evaluate oscillators.

1.1 Types of oscillators

There are many ways to implement oscillators, but most oscillators may be divided into two groups, namely relaxation oscillators and harmonic oscillators. A short description of their operating principles will now follow.

Relaxation oscillators are based on repetitively charging and discharging an energy-storing element such as a capacitor or an inductor. The process can be managed by for example transistor switches that turn on and off when the voltage over a capacitor or the current through an inductor reaches some threshold level. The switches change the circuit and cause the charging or discharging process of the energy-storing element to commence. The frequency of oscillation is determined by the magnitude of the charging current or voltage and a time constant that is dependent on the size of the energy-storing element and on the rest of the circuitry of the oscillator.

Harmonic oscillators, or LC oscillators, are based on amplifiers and filtering functions. A common way of implementing a harmonic oscillator is to employ a single-transistor amplifier and to use either parallel resonance or series resonance LC circuits (also called tanks) made of an inductor and a capacitor. The LC circuit has a center frequency defined by the values of the inductor and the capacitor:

$$f = \frac{1}{2\pi\sqrt{LC}} \tag{1.1}$$

Instead of acting as a circuit-changing switch as in relaxation oscillators, the transistor connected to the LC resonator acts as an amplifier that compensates the energy losses occurring due to the finite quality factors of the inductor and the capacitor. This results in an oscillator that produces sustained oscillations on (or close to, due to various parasitic effects) the center frequency of the LC resonator.

Harmonic oscillators are usually favored over relaxation oscillators due to their better spectral purity and frequency stability. However, the highest quality factors of inductors in modern semiconductor processes are only about 20, and thus it is still difficult to design low-noise harmonic oscillators. Inductors are also large consumers of silicon area, and it is not uncommon for the rest of an LC oscillator circuit to be smaller than the inductor in the LC resonator.

1.2 Criteria for oscillation

Oscillators can be designed in many different ways, but there are always some criteria that must be fulfilled in order for the oscillator to work properly. Basic oscillators can be modelled as a feedback system, shown in Figure 1.1.

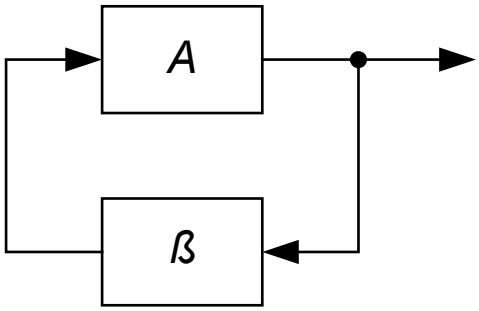

Figure 1.1. Block diagram of a feedback system.

In the block diagram, block A represents an amplifier and block β represents a feedback network that is connected from the output of the amplifier to its input. The criteria that such a feedback system must fulfil in order to oscillate have been neatly collected together as the so-called Barkhausen criterion [5]. When using the notations of the model in Figure 1.1, this criterion can be given as

$$A\beta = 1 \tag{1.2}$$

It can thus be divided into two parts, i.e. the magnitudes A and β and their phases must each fulfil separate criteria, here denoted as the magnitude criterion and the phase criterion.

1.2.1 Magnitude criterion

The magnitude criterion for oscillation states that the gain $A\beta$ of the oscillator loop must be equal to 1 during standard operation. In practice the loop gain has to be larger than 1 for the oscillator to begin to oscillate and for the oscillation amplitude to grow. The amplitude will eventually saturate due to device nonlinearities, reducing the loop gain to 1 and providing a signal with stable amplitude.

1.2.2 Phase criterion

The phase criterion for oscillation states that the phase shift of the oscillator loop must be a multiple of 2π. In other words $\arg(A) + \arg(\beta) = k2\pi$, where k is an integer. This means that signals at a certain point in the oscillator are summed with the same phase, causing a sum signal that is greater than any of the single signals. If the phase shift were to be an odd multiple of π, for example, the signals would have opposite phases and would cancel each other. In that case no oscillations could occur in the circuit.

1.3 Frequency controllability

When using an oscillator in radio devices, it is often desirable to perform channel selection by changing the frequency of the oscillator connected to a down-converting or up-converting mixer. This is where the simple single-frequency oscillator must be transformed into a device whose output frequency can be controlled through a dedicated

voltage (voltage controlled oscillator, VCO) or a dedicated current (current controlled oscillator, ICO). The manner of implementing the frequency tuning depends on the oscillator type.

A very common way of tuning traditional LC oscillators is to use variable capacitors (varactor). The varactor is connected to the oscillator's LC tank and a control voltage is applied over it. When a change in the output frequency is desired, the control voltage is changed, thus affecting the capacitance of the varactor. The total capacitance and thus also the center frequency of the resonator are changed, resulting in a new oscillator output frequency. The oscillator can also incorporate multiple varactors, with some meant for coarse tuning and others for fine tuning (see for example [6]). Some recent IC oscillator implementations (see for example [7]) have utilized completely digital tuning, thus effectively transforming the VCO into a digitally controlled oscillator (DCO).

Relaxation oscillators are usually tuned by changing the current that the oscillator consumes. This changes the current that charges the capacitor or the voltage that charges the inductor, and thus the frequency of the oscillator is also changed. This tuning scheme for relaxation oscillators usually provides a larger frequency tuning range than the use of varactors in LC oscillators does.

1.4 Effect of resonator quality factor on oscillator performance

When making harmonic oscillators, designers usually want to utilize resonators with the highest possible quality factors. This is because the quality factor has a clear impact on the frequency stability and the spectral purity of the oscillator. For traditional oscillators on silicon, a higher quality factor usually provides only improvements in oscillator performance. However, the matter is not so simple when designing oscillators that utilize resonators with very high quality factors, such as FBARs, crystals, and SAW resonators.

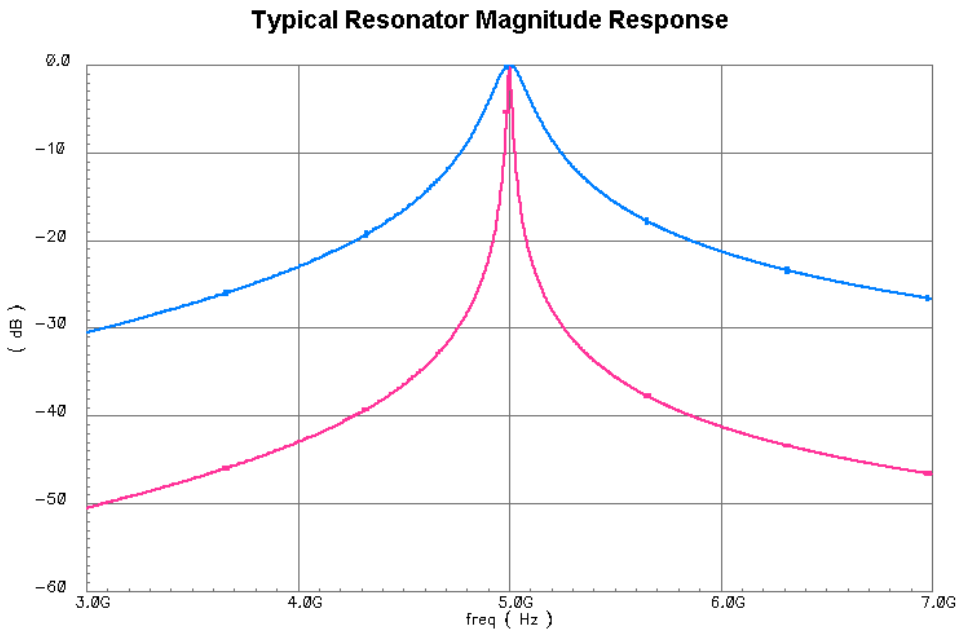

Figure 1.2. Effect of quality factor on resonator magnitude response. High *Q* (pink) and low *Q* (blue).

As is shown in Figure 1.2 for a 5-GHz resonator, a higher quality factor causes the 3-dB passband of resonators to become narrower. Because of this, the resonators filter out unwanted signals more effectively and preserve the wanted signal better. In oscillators this results in increased spectral purity. Changing the quality factor also clearly changes the phase response of resonators, as shown in Figure 1.3. The sharpening of the phase response has an effect on the phase noise or the frequency stability of the oscillator. This is because the phase shifts close to the resonance frequency become larger, and thus even small frequency changes are met with increasingly unacceptable deviations of the phase shift from the optimum 0 degrees at the resonance frequency.

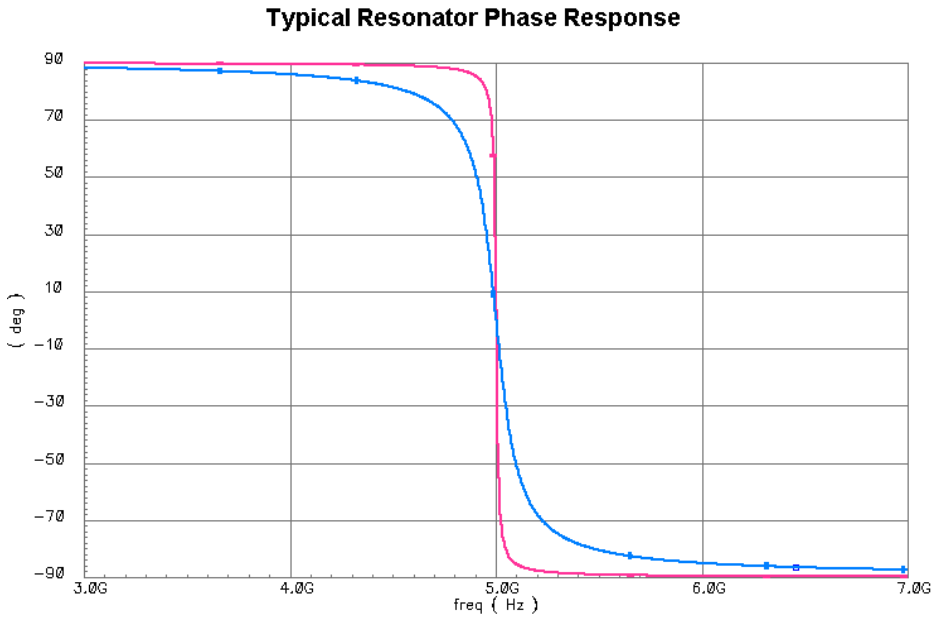

Figure 1.3. Effect of quality factor on resonator phase response. High Q (pink) and low Q (blue).

According to [8], the quality factor Q and phase noise L are directly linked to each other:

$$L(f_m) \propto \frac{2kT}{P_{Out}^2} \cdot \frac{1}{4Q^2} \cdot \frac{f_0^2}{f_m^2} \tag{1.3}$$

In other words, oscillator phase noise is inversely proportional to the quality factor of the resonator. Thus one should seek to maximize the resonator's quality factor when designing a high-performance low-noise oscillator.

1.5 Oscillator parameters

As with any other electronic devices, the performance of an oscillator and its suitability for inclusion in larger systems is evaluated through certain parameters. A short description of some of the most important ones is given below.

1.5.1 Oscillation frequency

The oscillation frequency f_0 or the fundamental frequency of an oscillator is defined as the frequency at which the main peak in the oscillator's output spectrum is

located. When speaking of gigahertz-range oscillators, for example, the oscillator's main output is located on a frequency in the gigahertz-range.

1.5.2 Frequency tuning range

The tuning range of an oscillator is defined as the distance between the lowest and highest output frequencies that the oscillator can produce. For RF oscillators it is usually given in MHz or GHz.

$$Tuning\ range = f_{0_{\max}} - f_{0_{\min}} \tag{1.4}$$

1.5.3 Tuning voltage or tuning current range

The tuning voltage (or current) range refers to the range of acceptable voltages or currents that can be applied to the tuning circuitry of an oscillator. The range can for example be given as 0 V to 3 V, or 2 mA to 5 mA.

1.5.4 Frequency tuning curve

The frequency tuning curve is a graphic representation of what happens to the oscillator's output frequency as the tuning voltage or current is swept through the acceptable range. It is usually desirable that the tuning curve is monotonic, i.e. that the output frequency constantly rises or constantly goes down as a function of the tuning voltage or current.

1.5.5 Power consumption

This measure tells how much power the oscillator drains from its power supply. It is usually given in mW.

$$P_{DC} = V_{CC} \cdot I_{CC} \tag{1.5}$$

1.5.6 Load resistance

The outputs of oscillators are usually loaded with some impedance, for example another circuit stage or a discrete load resistor. The load of the oscillator is usually designated as R_L, and a very common value for its resistance is 50 Ω.

1.5.7 Output power

This is the power that the oscillator delivers into its load resistance R_L. It is usually given in dBm, decibels referenced to 1 mW.

$$P_{Out} = \frac{V_{Out}^2}{R_L} \tag{1.6}$$

1.5.8 Frequency purity and harmonic content

The output spectrum of real oscillator implementations consists of peaks at the fundamental frequency and at many harmonic frequencies (multiples of the fundamental), all of them also containing side lobes that make the peaks wider than a discrete line. The lower the power levels of the harmonic frequencies, the purer the oscillator's output.

One way to quantify frequency purity is to measure the power of the harmonics and compare them to the power of the fundamental output frequency component. The power levels are then usually given in dBc, meaning decibels with reference to the carrier at f_0. Another common measure for frequency purity is total harmonic distortion (THD), defined in the manner shown in (1.7). In the formula, A_1 refers to the amplitude of the fundamental frequency component and the other terms A_i refer to the amplitudes of the harmonic frequency components:

$$THD = \frac{\sqrt{A_2^2 + A_3^2 + ...}}{A_1} \cdot 100\% \tag{1.7}$$

1.5.9 Spurious frequencies

In addition to harmonic components, the oscillator's output may sometimes contain components that are situated on frequencies other than multiples of the fundamental frequency. These are referred to as spurious frequencies.

1.5.10 Phase noise

Phase noise is a measure of the frequency stability of an oscillator. It is defined as the ratio of the output signal power at a certain offset f_m from the carrier f_0 and the power of the carrier, both within a 1-Hz bandwidth. It is usually given in dBc/Hz.

$$L(f_m) = 10\log\frac{P(f_m)}{P(f_0)} \tag{1.8}$$

1.5.11 Pushing figure

The pushing figure of an oscillator gives the dependence of the output frequency on the supply voltage. It is usually given in MHz/V.

$$Pushing\ Figure = \frac{\Delta f}{V_{CC_{\max}} - V_{CC_{\min}}} \tag{1.9}$$

1.5.12 Pulling figure

The pulling figure indicates how dependent the oscillator's output frequency is on the value of the load impedance.

$$Pulling\ Figure = \frac{\Delta f}{R_{L_{\max}} - R_{L_{\min}}} \tag{1.10}$$

2 FBAR Devices in Frequency-Controllable Oscillators

Utilizing FBAR devices in implementing integrated oscillators is a novelty, especially if the output frequency is controllable. Very little work on FBAR oscillators has been done so far, but a few implementations now exist in the published literature. This chapter gives an overview of FBAR devices, discusses the implications for selection of suitable oscillator architecture, and reviews FBAR oscillators that have been previously published.

2.1 What is an FBAR?

The Film Bulk Acoustic Resonator (FBAR) is a device that converts electrical energy into mechanical energy and vice versa at its input/output electrodes. Since the FBAR is part of the family of Bulk Acoustic Wave (BAW) devices, the mechanical energy "travels" through the bulk of the material as a longitudinal wave, not through the surface as in Surface Acoustic Wave (SAW) devices [9]. A cross-section of an FBAR built on top of an integrated circuit is shown in Figure 2.1 [1].

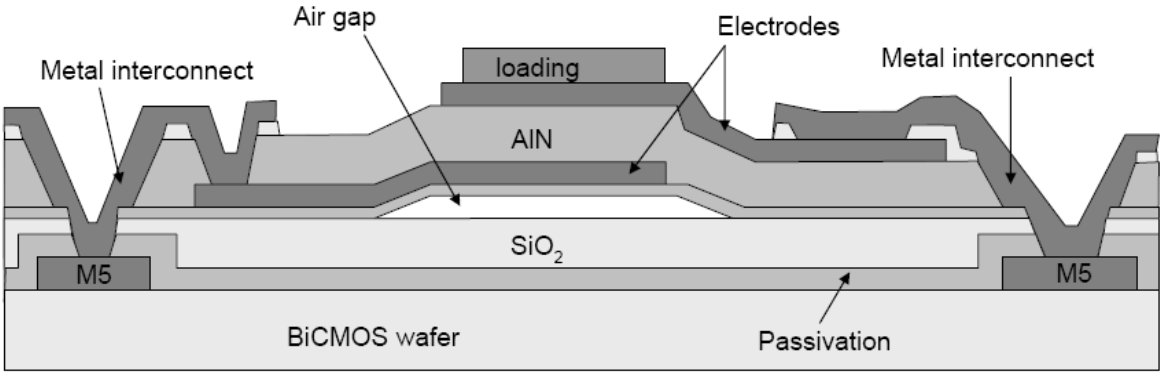

Figure 2.1. Cross-section of an above-IC FBAR.

The FBAR device itself is a sandwich consisting of a piezoelectric (in this case aluminium nitride, AlN) between two electrodes that serve as input and output and that can be connected to other circuitry. When connected on top of an IC, as in Figure 2.1, the electrodes are attached to interconnects that lead to the highest metal layer of the integrated circuit. The FBAR is acoustically isolated from the BiCMOS wafer by creating an air gap between the FBAR and the IC.

The piezoelectric material of the FBAR reacts differently depending on the frequency of the electrical signal applied to the FBAR. Around some frequency the magnitude of the FBAR's impedance reaches its minimum, which means that the acoustic wave travels through the physical material in the most efficient way. This frequency is called the series resonance frequency f_s, sometimes simply called the resonance frequency. On the other hand, the magnitude of the FBAR's impedance reaches its maximum around another frequency. At this frequency the piezoelectric hardly responds at all, and thus no acoustic wave transfers energy through the FBAR. This frequency is called the parallel resonance frequency f_p, sometimes also called the anti-resonance frequency. The situation is illustrated in Figure 2.2.

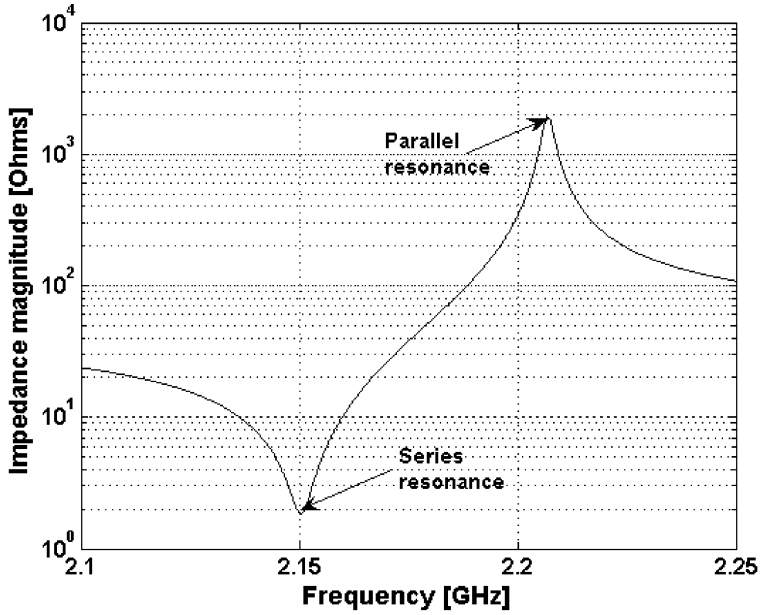

Figure 2.2. The frequency response of a typical FBAR. Series resonance frequency f_s and parallel resonance frequency f_p shown.

FBAR devices have been manufactured already for many years, and clear advances have been made in quality factor and yield. Table 2.1 shows a brief comparison of the characteristics of some recent FBARs. Since the present oscillator utilizes series resonance, the table lists frequency and quality factor values related to series resonance. The quality factors of these resonators vary from a few hundred to just over one thousand, depending on the electrode material and the thickness and the area size of the piezoelectric material. They are thus considerably higher than the quality factors achievable for LC resonators in modern IC processes.

Table 2.1. Some recently reported FBAR devices.

Reference	f_S [GHz]	Q_S	Size [mm^2]
[10]	1.1	386	0.058
[11]	1.9	832	-
[12]	1.9	1200	0.01
[13]	5.0	290	-
[14]	1.9	1025	-
[15]	4.9	300	-

The electrical characteristics of the FBAR can be modelled by using the Butterworth-Van Dyke (BVD) equivalent circuit usually employed when modelling quartz crystals. However, the impedance locus of the FBAR deviates from that produced by this model, and therefore a more accurate version has been proposed in [16]. The difference between this new Modified Butterworth-Van Dyke (MBVD) model of the FBAR and the traditional BVD model is the addition of resistor R_0 in series with plate capacitance C_0 (see Figure 2.3). The motional resistance R_m and the electrode resistance R_s are the main factors degrading the intrinsic quality factor of the FBAR.

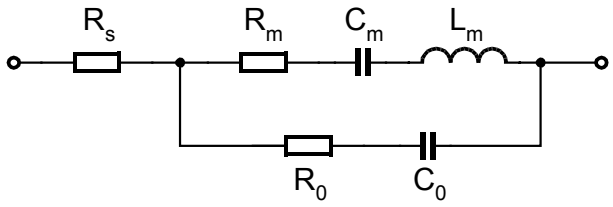

Figure 2.3. The MBVD model used to describe the electrical performance of FBARs.

The meaning of each component in the MBVD model is explained in the following:

- R_s is the resistance of the electrodes that connect the FBAR to the IC
- R_m, C_m, and L_m are components modeling the electromechanical response of the FBAR
- R_0 is the plate resistance
- C_0 is the plate capacitance, and its value depends on the size of the FBAR's physical footprint

It is customary to first fabricate stand-alone FBAR devices and then to extract a model for them (for more information on extracting the MBVD model, see [16]). The resonator is included in electrical simulations as the lumped-element MBVD model, and in the above-IC case, it is later built on top of the fabricated SiGe oscillator circuit through post-processing steps.

2.2 FBAR frequency tuning and circuit selection

The major problem with implementing frequency tuning in circuits utilizing FBAR devices is that the resonator itself cannot be changed. Similarly to quartz crystals, it is possible to change the FBAR's parallel resonance frequency by connecting a capacitor in parallel, or to change its series resonance frequency by connecting a capacitor in series with the FBAR. In both cases, the changed resonance frequency moves closer to the other resonance frequency. This limits the tuning possibilities to a small section of the initial distance between the series and parallel resonance frequencies.

Another way of realizing frequency tuning may be arrived at by considering the FBAR as a filtering component, with the Q-factor of the FBAR determining the bandwidth of the filter. For high-order LC circuits such as the model of the FBAR, the definition of Q is not as straightforward as it is for simple LC tanks. In our case we will assume that the Q of the series resonance is the ratio of the impedance of one of the reactive components C_m or L_m and the total sum of all resistances in series with it. For the parallel resonance, Q is the ratio of the energy in the reactive components and the energy dissipated in the resistive components.

The two Q-factors can be different and can be independently controlled with external components. For example, if R_s in Figure 2.3 is small (in the order of a few ohms or tens of ohms), it affects only the Q-factor of the series resonance. This is because the impedance of the circuit at parallel resonance is much larger. In a similar way, if we connect a large resistor R_p (in the order of kiloohms) in parallel to the FBAR (shown with broken lines in Figure 2.4), it affects only the parallel resonance since the impedance of the series branch at series resonance is very small.

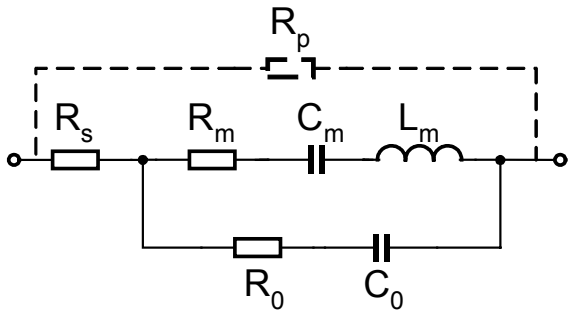

Figure 2.4. MBVD model with external resistor R_p attached.

The magnitude of the FBAR's impedance versus frequency is plotted in Figure 2.5 for different values of R_s and R_p. The magnitude of the impedance is plotted when R_s and R_p are independently varied. When R_s is changed, R_p is kept at 100 kΩ, which is approximately equivalent to an open circuit; when R_p is varied, R_s is kept at a nominal value of 0.8 Ω. As can be expected, the impedance varies significantly between the resonance frequencies f_s and f_p in all cases (~ min. 2 Ω at series resonance and max. 2 kΩ at parallel resonance for the FBAR without any external circuitry). The variation of R_s has noticeable effect only around the series resonance, whereas the variation of R_p affects the response only around the parallel resonance.

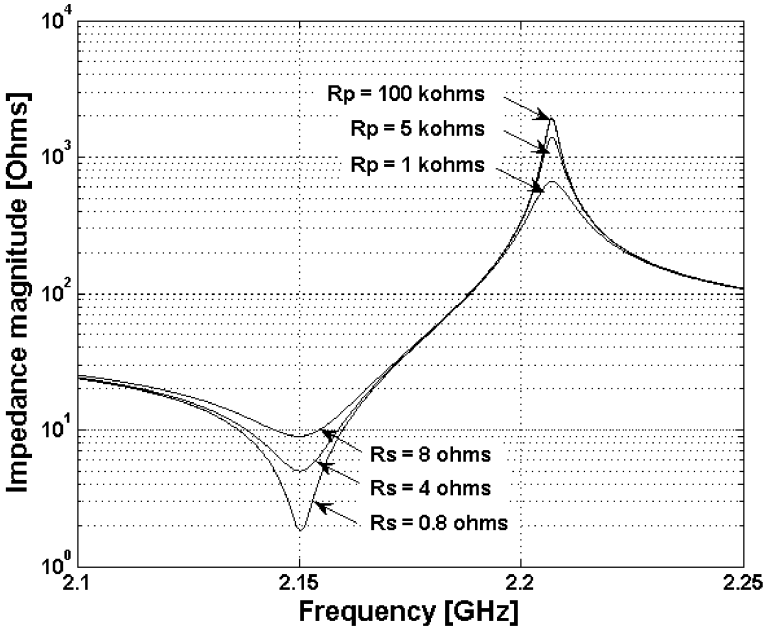

Figure 2.5. Frequency response of the FBAR lumped-element model with the effect of independently varying R_s and R_p shown.

From the above considerations it follows that we are able to tune the Q-factor at series or parallel resonance by adding an appropriate resistor. From a practical point of view, it is easier to operate with series resonance, because in this case we need a resistor of only a few ohms. In contrast, if we use parallel resonance the needed resistor is very large. The reduction of Q must of course be moderate in order to preserve the good phase noise performance expected of an FBAR oscillator.

A major factor guiding the choice of oscillator architecture is thus that the oscillator should utilize the resonator in the series resonance mode. In this case the FBAR must be connected in a low-impedance part of the circuit, so that the surrounding

impedances are low enough not do degrade the series resonance Q of the FBAR too much. A good candidate for the architecture is a Butler-type oscillator, the block diagram of which is shown in Figure 2.6. The FBAR is represented as a series-resonance circuit and is connected between the output of a common-collector (CC) amplifier and the input of a common-base (CB) amplifier. Further discussion of this architecture is found in chapter 3.

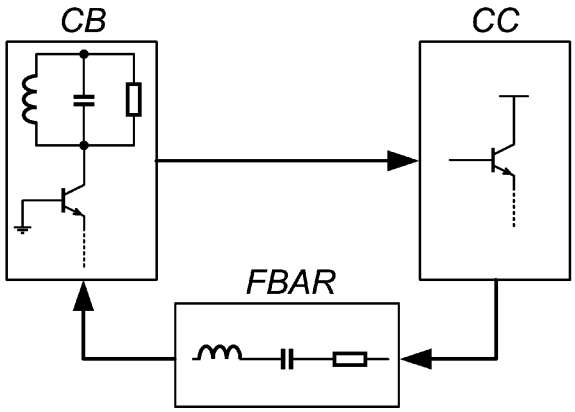

Figure 2.6. Block diagram of the suggested oscillator structure.

2.3 Earlier FBAR oscillator implementations

As mentioned earlier, oscillators are often designed by using LC resonators. In IC implementations, the resonator quality factors are usually quite low, mainly because of the low quality factor of available inductors. Thanks to recent developments, it has become possible to utilize the high-Q FBAR in the design of integrated circuits. The FBAR can also be used in non-IC discrete implementations. Because the FBAR does not conduct DC current, some oscillator topologies that require the conduction of DC current through the resonance circuit are ruled out. However, there are still many different circuit architectures that can be used for realizing FBAR oscillators.

To facilitate a comparison between previously published FBAR oscillators, a commonly used figure of merit (FOM) is employed. In the FOM equation below, the term $L\{\Delta f\}$ stands for phase noise at a given offset Δf away from f_0, the center frequency of the oscillator:

$$FOM = L\{\Delta f\} - 20\log(\frac{f_o}{\Delta f}) + 10\log(\frac{P_{DC}}{1mW}). \quad (2.1)$$

Comparisons between oscillators are always difficult to make, though, and in this case, the important feature of frequency tunability in some FBAR oscillators is not taken into account. At any rate, the previously published circuits and some of their most important performance parameters are listed in Table 2.2.

Table 2.2. Comparison of FBAR oscillators.

Reference	f_0 [GHz]	Power	Tuning range [MHz]	Best PN @1 MHz [dBc/Hz]	FOM [dB]	Technology
[12]	1.9	1 V / 0.3 mA	0	-140	-211	0.18-µm CMOS
[15]	5.0	-	0	-120	-	Discrete
[17]	2.0	3.3 V / 35 mA	2.5	-150	-195	Bipolar
[18]	1.9	0.43 V / 0.2 mA	0	-140	-216	0.13-µm CMOS
[19]	1.1	-	0.2	-123	-	Discrete

In [15] the oscillator is built on a printed circuit board (PCB), and the FBAR is wirebonded to the board. The oscillator core is based on a common-base architecture, and the specialty of this particular implementation is the very low temperature coefficient of frequency of the FBAR. This means that the resonance frequencies of the FBAR are very immune to changes in ambient temperature. As a downside, the oscillator suffers from poor phase noise at high offsets.

The oscillators described in [12] and [18] are based on the Pierce structure and feature very low power consumption. The separate FBAR is in each case connected to the CMOS chip with bondwires, which are very short in order to minimize inductance in the interface between the chip and the FBAR.

The core schematic of the oscillator in [18] is shown in Figure 2.7. In the circuit, transistors M_1 and M_2 together with capacitors C_1 and C_2 form a negative resistance that offsets the resistive losses in the FBAR and thus cause oscillation.

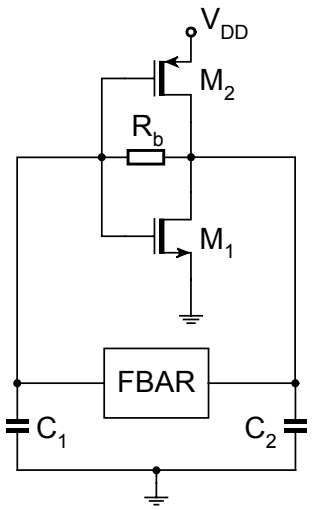

Figure 2.7. Schematic of a Pierce-based FBAR oscillator.

The circuit in [19] and shown in Figure 2.8 is a Colpitts-based PCB oscillator, with the FBAR again wirebonded to the rest of the circuitry. Some frequency tuning is achieved by applying a DC control voltage that changes the electrical field in the piezoelectric film of the FBAR and alters the resonance frequencies. However, the achieved frequency tuning range is very small.

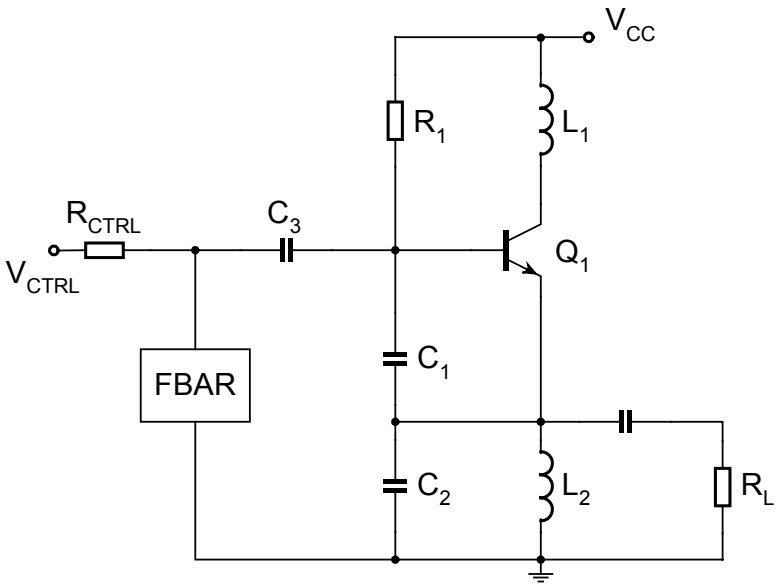

Figure 2.8. Schematic of a Colpitts-based FBAR oscillator with tuning.

The VCO discussed in [17] represents the best published effort to date to achieve frequency tuning in an FBAR oscillator. The circuit is based on a common-collector architecture, with the FBAR being bonded to the oscillator using 1-mil wires. The frequency tuning range of 2.5 MHz is achieved with the help of a varactor.

When examining the performance of these oscillators it can be seen that frequency tuning range so far has been very low. Such tuning ranges cannot really be exploited in multi-channel applications, but they are good for fine tuning. Two of the implementations have been very successful in capitalizing on the power-saving potential offered by the FBAR. Due to its high quality factor (and thus its low losses) the FBAR does not need as much replenishing energy as high-loss LC resonators usually do. It is also important to note that none of the circuits listed in the table utilize an above-IC FBAR, but rather the circuits, either integrated or discrete in themselves, are connected to the FBAR through wirebonding.

3 The Present Oscillator Architecture

This chapter discusses the particular oscillator circuit topology that was chosen for implementation of the FBAR VCO and the LC VCO used as a comparison point. We will take a brief look at its prior development and variations, its operating principle, and the method of frequency tuning. Because output buffers are often needed for measurement and system integration purposes, two simple buffers that can be used with this oscillator will be presented.

3.1 Development history

Since Butler introduced his two-valve oscillator architecture based on vacuum tubes and a crystal resonator, many transistorized variations of the circuit have been proposed. The addition to the basic structure of an amplitude-regulating stage was described in [20], with another type of amplitude-limiting amplifier increasing oscillator frequency stability and spectral purity discussed in [21]. A solution reducing the strain placed on the frequency-determining crystal was proposed in [22], and a way of introducing digital frequency control by directly adjusting the resonance circuit within the oscillator was shown in [23]. More recently, an IC implementation of the two-transistor architecture using an LC resonator was proposed in [24] and further investigated in [25]. Here the analog frequency control circuitry is detached from the resonance circuit, thus avoiding harmful effects of high-frequency interference being inserted directly at the resonator. The present architecture (LC implementation in Figure

3.1, FBAR implementation in Figure 3.2) is a further development of this last-mentioned circuit.

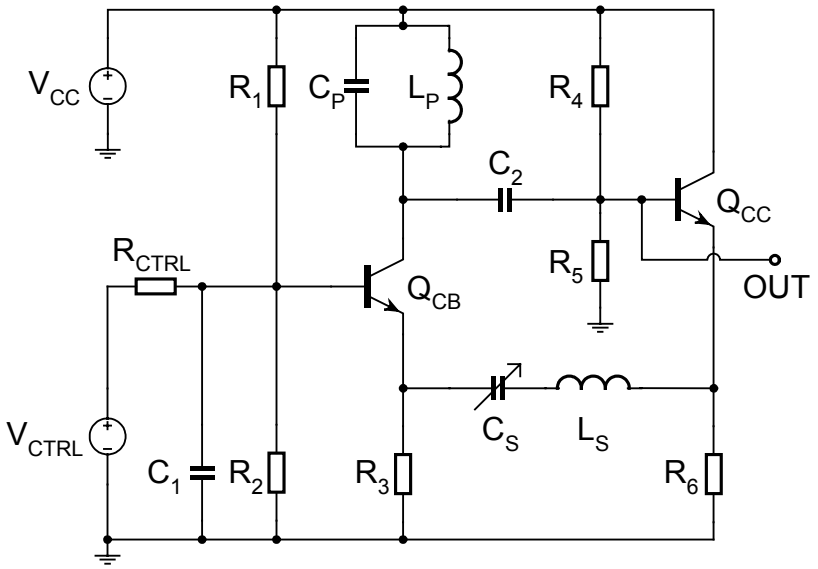

Figure 3.1. LC implementation of the present oscillator architecture.

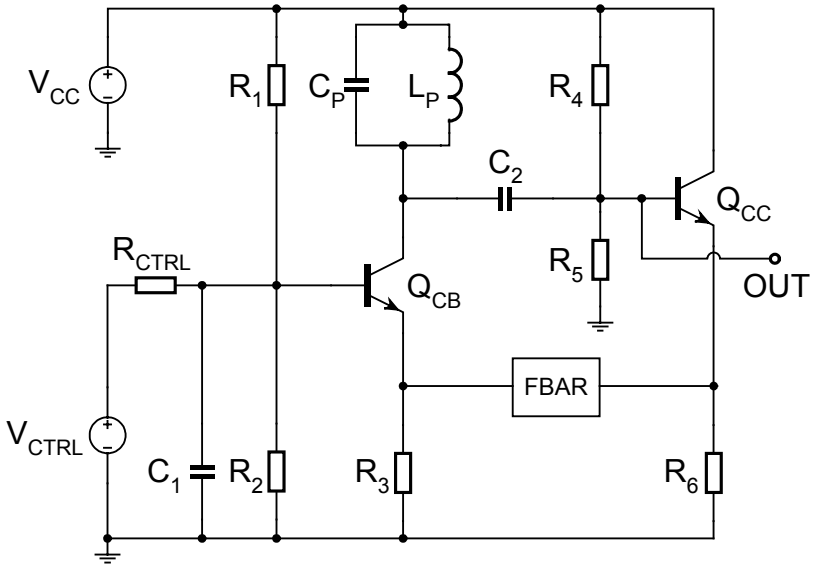

Figure 3.2. FBAR implementation of the present oscillator architecture.

Compared to [24], the main novelty in the present architecture is the insertion of a parallel resonance LC tank between the power supply and the collector of the common-base transistor. Inserting the tank increases the spectral purity of the oscillator and provides a path to AC ground for possible spurious signals created in the oscillator core. In addition it eliminates the voltage drop and noise that would be caused by the bias

resistor in its stead. It is possible to implement the oscillator without this parallel resonator. However, unless IC chip area is the most critical factor guiding the design of the oscillator, the many benefits obtained by using the parallel resonance circuit instead of a collector bias resistor outweigh the cost of increased layout size.

3.2 Operating principle of the LC VCO

The VCO core consists of a common-base amplifier connected in loop configuration with a common-collector amplifier. This loop provides positive feedback and together with the resonators causes the circuit to oscillate. The main voltage amplifier is the common-base amplifier, which has high output impedance and low input impedance. The common-collector amplifier has high input impedance and low output impedance, and thus it serves as an impedance-matching buffer between the output and the input of the common-base amplifier.

Many LC oscillators require a resonator that operates in the parallel-resonance mode. This means that the circuit usually assumes the conduction of DC current through the resonator. However, in the present circuit no conduction of DC current is assumed through the series resonance circuitry. Therefore the series resonance LC tank can later be replaced by an FBAR that does not conduct any DC current.

It will be remembered that in order for the circuit to oscillate, it has to fulfill the Barkhausen criterion. We will now see in what manner the magnitude criterion and the phase criterion for oscillation are satisfied.

3.2.1 Magnitude criterion

The voltage gain of a common-base amplifier is usually significantly larger than 1, and the voltage gain of a common-collector amplifier is usually around 0.9 to 1. In the case of this oscillator, that voltage gain is only 0.7 – 0.8, because the load impedance of the common-collector amplifier is very low close to the resonance frequency of the series resonator. The loop gain of this oscillator is the product of these two voltage gains and is much larger than 1 at frequencies close to the resonance of the series LC tank, thus making oscillation possible. During stable operation, the loop gain is reduced to 1 because of transistor nonlinearities.

3.2.2 Phase criterion

The fully-LC implementation of the oscillator core basically consists of two bandpass stages or tuned amplifiers, namely the common-base amplifier together with the parallel resonator, and the common-collector amplifier together with the series resonator. These bandpass stages have continuous phase responses that set out from +90 degrees at very low frequencies and that proceed to -90 degrees at very high frequencies. Both of the phase responses are zero at the respective resonance frequencies. The oscillator oscillates on the frequency at which the sum of these two phase responses is zero, or where they cancel each other. An illustration of the situation is seen in Figure 3.3. In the plot, CB refers to the common-base amplifier, while CC refers to the common-collector amplifier.

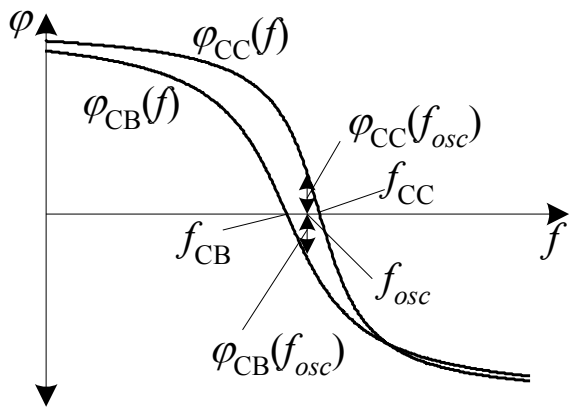

Figure 3.3. Oscillation frequency as a function of stage phase responses in a fully-LC implementation.

3.2.3 Frequency tuning method

Frequency tuning in LC oscillators is usually realized by connecting a control voltage directly at the varactor that is part of the LC resonator. A more unusual manner of tuning is used in this VCO implementation, bringing with it both advantages and disadvantages. The tuning mechanism used in this oscillator consists principally of two portions.

First, the tuning is provided by changing the bias point of the common-base amplifier. This causes a change in the emitter voltage, and in fully LC implementations it

consequently changes the voltage over the varactor located in the series feedback loop. This changes the resonance frequency of the series resonance LC tank.

Second, the loaded Q-factor of the series resonator changes as the bias current I_C and thus the input resistance R_{inCB} [26] of the common-base amplifier is changed through variations of the tuning voltage:

$$R_{inCB} = \frac{1 + r_b / r_\pi}{g_m \left(1 + 1/\beta_0\right)} \approx \frac{1}{g_m} = \frac{V_T}{I_C} \tag{3.1}$$

This changes the slope of the phase response of the series resonator and consequently affects the total zero-phase-shift frequency of the VCO core loop. These effects together cause a change in the oscillation frequency of the circuit.

3.3 Operating principle of the FBAR VCO

The operation of the FBAR VCO is based on the same principles as the operation of the LC VCO detailed in the previous subsection. The main differences between the two are in the phase condition and in the frequency tuning mechanisms.

3.3.1 Magnitude criterion

As in the LC implementation, the loop gain is higher than 1. This is because the gain of the common-base amplifier is unaffected, and the common-collector amplifier is still loaded by a low impedance at the resonance frequency of the series resonator, in this case the FBAR.

3.3.2 Phase criterion

With respect to the phase criterion, the situation is more complicated in the FBAR-version of the oscillator. Similarly to the LC implementation, however, the loop again contains elements that produce phase shift. The main contributors are the parallel LC tank and the FBAR, with coupling capacitors acting as more minor influences. The circuit will oscillate on the frequency where the total phase shift in the core loop is a multiple of 2π.

3.3.3 Frequency tuning method

The main challenge with using BAW, SAW, and quartz crystal high-*Q* resonators in tunable oscillators is usually the drastic reduction of available frequency tuning range. The largest frequency tuning previously reported for an FBAR oscillator is 0.13 % [17]. This is too small for beneficial use of the VCO in multi-channel applications, and the small tuning range can mainly be exploited in fine tuning. Thus it becomes of primary importance to look for ways in which this limitation can be overcome.

In an FBAR implementation of the oscillator, a varactor could be connected in series with the FBAR. The varactor would then be used to make small changes in the series resonance frequency of the FBAR. Due to there not being a stable DC point between the varactor and the FBAR, however, some additional measures would have to be taken in circuit design. Instead of doing so, the tuning of the present FBAR oscillator is investigated and later implemented without a varactor.

As a basis for the theoretical considerations of frequency-tuning behavior, Figure 3.4 shows the simulated tuning curve of the single-ended version of the FBAR VCO, when the used power supply voltage is 2.4 V. Other details of the circuit are given in chapter 5.

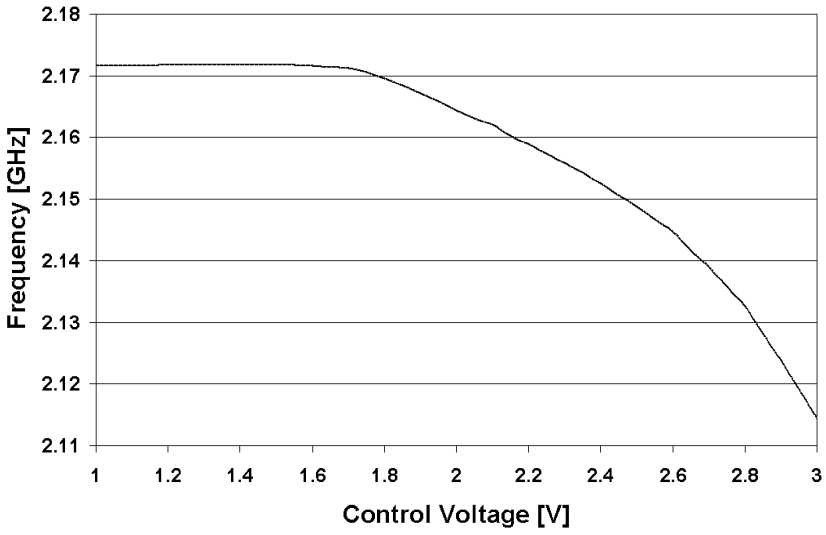

Figure 3.4. Simulated frequency tuning curve of the single-ended FBAR VCO.

To explain the extension of the tuning range, it is necessary to consider the mechanisms of oscillation in the circuit in more detail. Relying upon the Barkhausen criterion for oscillation we see that the exact value of the oscillation frequency is defined

by the phase condition. This is the frequency at which the total phase shift through the loop is equal to 0 or a multiple of 2π. In the present circuit the largest phase variations occur around the resonance frequencies of the FBAR. Additional phase variation takes place because of the parallel LC tank, transistor capacitances, and coupling and bypass capacitors. Since the parallel and series resonance frequencies of the FBAR are very close to each other, these additional phase shifts can be considered as constant within this narrow frequency area.

As shown above in (3.1), varying the bias point of the common-base amplifier has two effects: the altered value of g_m results in changed gain and changed common-base stage input resistance R_{inCB}. At lower control voltages, g_m and collector current I_C are small. This leads to the gain of the common-base stage not being large enough to sustain oscillation. At higher control voltages the gain of the common-base stage is sufficient for oscillation to appear, but the total loop gain doesn't increase proportionally. This is because the low input resistance of the common-base stage decreases the transfer ratio between the common-collector and common-base stages.

More importantly, the input resistance R_{inCB} of the common-base stage plays a significant role in defining the oscillation frequency. This is because it together with the FBAR determines the variation of the phase shift that occurs in the circuitry between the common-collector and common-base stages. The simplified model of this circuitry is shown in Figure 3.5. The phase of the transfer function between the common-collector and common-base stages for three different values of R_{inCB} is plotted in Figure 3.6. For the VCO control voltages 0.8, 1.6, and 2.4 volts, the used input resistances R_{inCB} are 20, 4, and 1.6 ohms, respectively (this data is based on simulations of the common-base stage). The output resistance of the common-collector stage is approximated as 6 ohms. For details on the FBAR model, please see chapter 5.

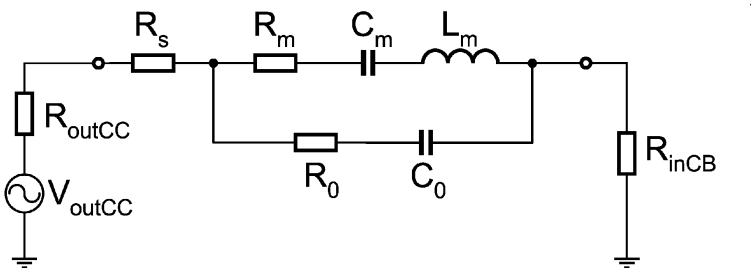

Figure 3.5. Model for simulating feedback loop phase response.

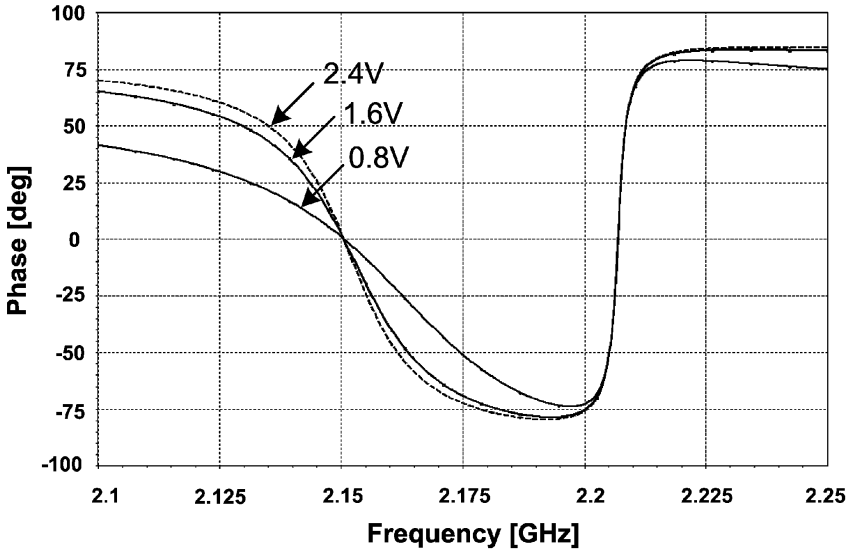

Figure 3.6. Phase response of the feedback loop with V_{CTRL} = 0.8, 1.6, and 2.4 volts.

In Figure 3.6, the zero-phase-shift point for all curves is exactly at the series resonance frequency (and also at the parallel resonance frequency, but this is irrelevant to our considerations) of the FBAR. However, the oscillations occur at a frequency different from this point due to the phase shift in the other parts of the oscillator.

This model is also not sufficient for explaining the tuning mechanism of the circuit. From simulating the oscillator it follows that the maximum variation of the output frequency occurs at control voltages above 1.7 V (see Figure 3.4), and at the same time Figure 3.6 gives the opposite conclusion. This means that there is another reason for the expansion of the tuning range.

We will now simulate the frequency behavior of the loop gain, and for this purpose we need to break the loop. We choose the output of the common-collector stage as an appropriate place to do so. In order to preserve the conditions at this output after breaking the loop, the common-collector stage is loaded with the FBAR in series with the input resistance of the common-base stage. The relevant portion of the oscillator circuit is shown in Figure 3.7. The magnitude and phase response at four different control voltages are shown in Figure 3.8 and Figure 3.9.

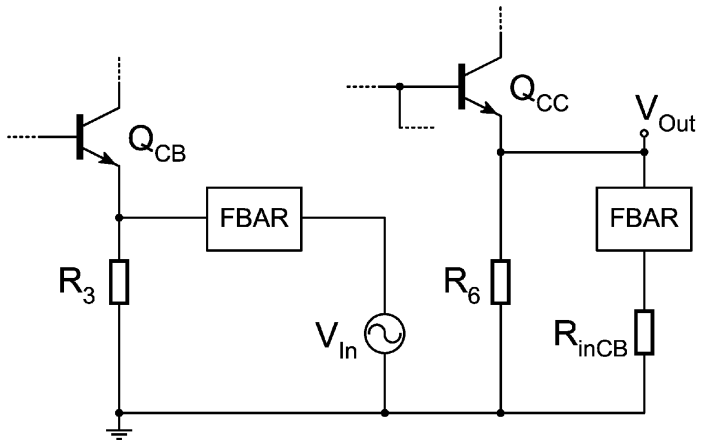

Figure 3.7. Circuit for loop magnitude and phase response simulation.

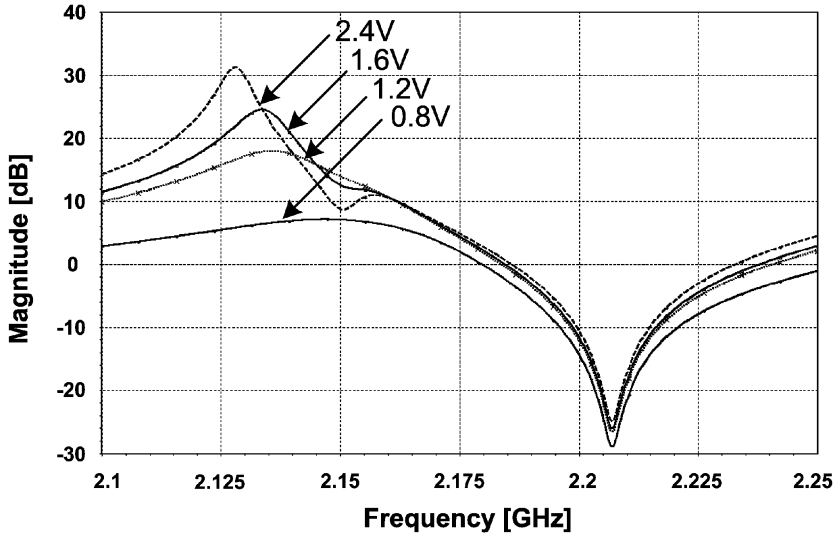

Figure 3.8. Magnitude response of the oscillator's core loop with V_{CTRL} = 0.8, 1.2, 1.6, and 2.4 volts.

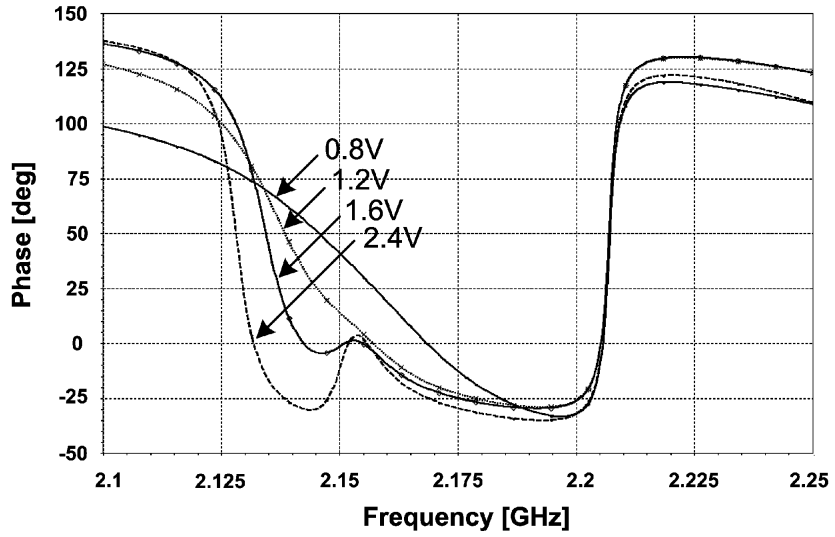

Figure 3.9. Phase response of the oscillator's core loop with V_{CTRL} = 0.8, 1.2, 1.6, and 2.4 volts.

From the phase response in Figure 3.9 we see that a second minimum appears as the control voltage increases. This happens when the input resistance R_{inCB} is very small and is comparable to the loss resistances of the FBAR. A significant effect of this second minimum is that it moves the zero-phase point of the loop to a lower frequency, thus extending the tuning range. An additional interesting observation is that the maximum of the phase between the two minima is located very close to the series resonance frequency of the FBAR.

The reason for this second minimum to appear is the interaction between the impedances in the oscillator's core loop. When the series resistance R_{inCB} is large, the load of the common-collector stage is in fact approximately equal to R_{inCB} around the series resonance frequency. When R_{inCB} is small (for example at control voltages greater than 1.6 V it is comparable to the resistances in the equivalent circuit of the FBAR), the load of the common-collector stage is the FBAR with a small increase in the form of series resistance R_{inCB}. This total impedance is transformed at the input of the common-collector stage as a larger impedance, but the series resonance still exists. Then it appears in parallel to the load of the common-base stage and further changes the imaginary part of the input impedance of the common-base stage. Thus the equivalent input impedance of the common-base stage around the series resonance is not only the resistive R_{inCB}, but rather it also has a significant imaginary part that affects the phase variation of the loop gain.

As a conclusion we can say that the reason for a wider tuning range is the variation of R_{inCB}, but the mechanism of extension is more complicated and cannot be explained merely by a change in the Q of the FBAR. It must also be borne in mind that the approximated results above have been arrived at by breaking the oscillator loop. This method produces some inaccuracies, because it is very difficult to recreate the exact loading conditions at the breaking point. This accounts for the difference between the simulated tuning curve in Figure 3.4 and the conclusions based on the phase curves in Figure 3.6. From Figure 3.9 it follows that the rapid change of frequency must appear at lower control voltages (1.2 to 1.3 V) than those in Figure 3.4 (1.6 to 1.7 V). At any rate, these considerations are a satisfactory estimation explaining the oscillator's operating mechanism.

The slope of the phase response at the zero-crossing point changes when altering V_{CTRL}, as shown in Figure 3.9. This slope is reflected by Q. Furthermore, the change of the quiescent point of the common-base stage changes the noise generation of this stage. Due

to these reasons we can expect variation in the phase noise when tuning the circuit, a matter later confirmed by the measurement results.

3.4 Output buffering

A buffer is usually inserted between the oscillator core and the load impedance in order to detach the load from the other circuitry and in order not to disturb the operation of the oscillator core too much. In this oscillator architecture, the optimum place to connect the buffer is the collector of the common-base stage, since the signal there has the highest amplitude and the best spectral purity. Because the load impedance is 50 ohms and the impedance at the collector is relatively high, the buffer needs to have high input impedance and low output impedance. In other words the buffer has an impedance-converting function in addition to separating the core from the load.

In basic single-ended applications, one of the simplest solutions for achieving the necessary buffering function is the common-collector amplifier, shown in Figure 3.10.

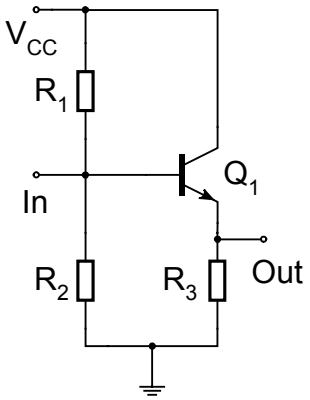

Figure 3.10. A common-collector amplifier used for output buffering.

The voltage gain of a common-collector buffer is usually around 0.9 - 1. Because the signal at the collector of the common-base amplifier has high amplitude, the small reduction in signal magnitude at the output of the buffer (and thus the output of the VCO) is not critical. A coupling capacitor is usually used between the output of the buffer and the load impedance.

Some communication system architectures require differential oscillator signals, but the signal in this VCO core is inherently single-ended. In this case, the necessary buffering will have to provide single-to-differential conversion in addition to impedance

conversion. One possible way of realizing these functions is to utilize a differential amplifier and two common-collector amplifiers, as shown in Figure 3.11.

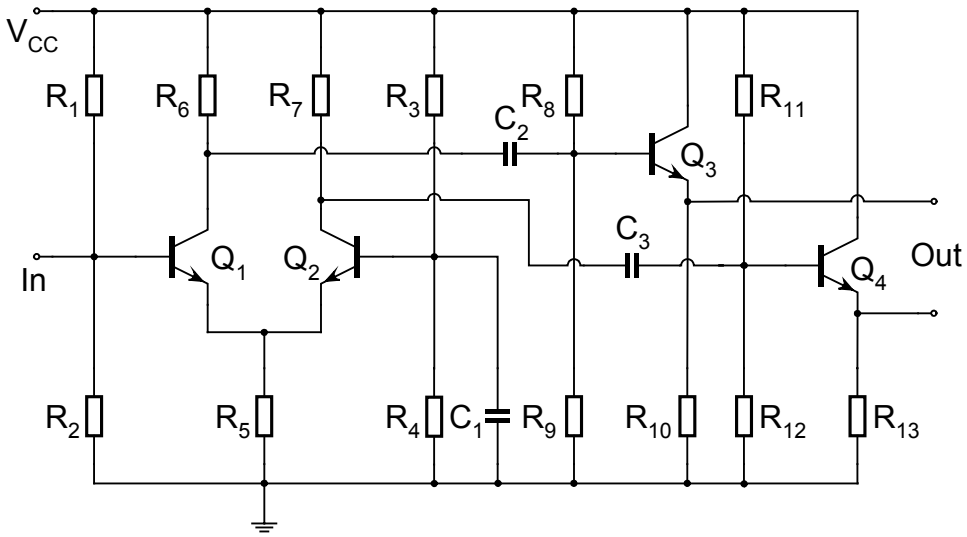

Figure 3.11. Differential amplifier and common-collector amplifiers used for obtaining a differential output signal.

Here the VCO core signal is connected to one input of the differential amplifier, with the other input AC grounded. The differential amplifier provides a differential output, where the two signals have a phase difference of approximately 180 degrees. Because the amplifier has high output impedance, both outputs are attached to common-collector buffers with high input impedance and low output impedance. The 50-ohm load impedance is then connected to the outputs of these common-collector buffers through coupling capacitors at the output.

4 A 2.1-GHz LC VCO in 0.25-µm SiGe BiCMOS

This chapter presents the design and measurements of a 2.1-GHz LC VCO that was designed as a testbench for a similar FBAR VCO utilizing the same architecture. The circuit is based on the architecture that was presented in chapter 3. The electrical simulations were performed with Cadence IC 4.4.6 and Spectre, the layouting was done with Cadence Virtuoso, and DRC and LVS checks were performed with Mentor Calibre software. Some parasitics of the circuit were manually estimated and included in final simulations.

The circuit was sent for fabrication in a 0.25-µm BiCMOS process of ST Microelectronics in November 2003. The silicon dies arrived for measurement in May 2004. Measurements were performed by using a Cascade Microtech 9000 probe station, an HP4352S signal source analyzer and a Rohde & Schwarz FSEM 26.5-GHz spectrum analyzer.

4.1 Schematic diagram

The schematic of the implemented LC VCO with component values included is shown in Figure 4.1.

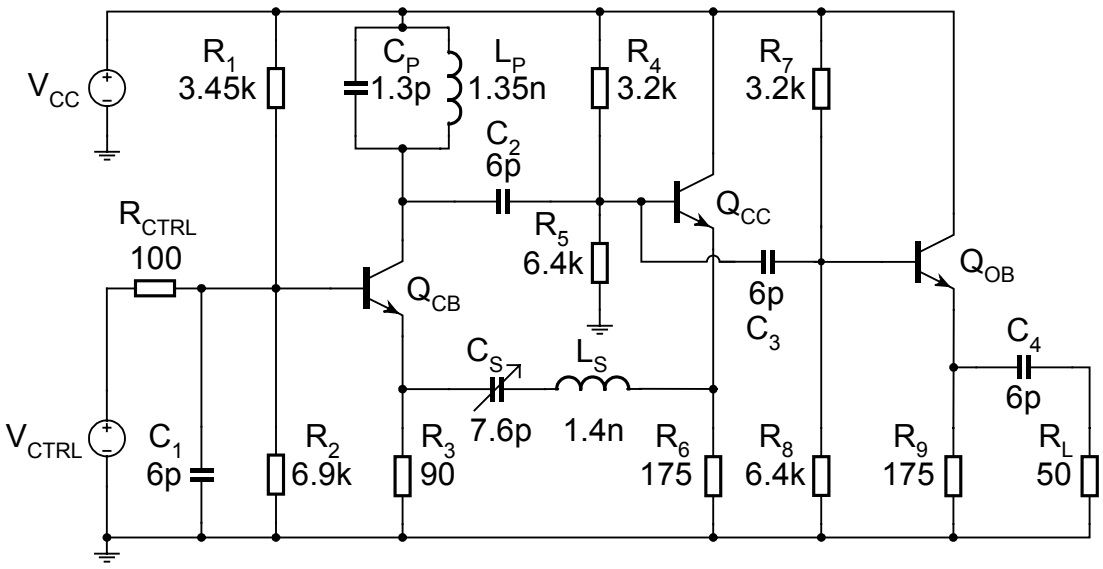

Figure 4.1. Schematic of the 2.1-GHz LC VCO.

The transistors of the circuit were realized as several unit transistors connected in parallel to each other, each transistor having two collectors and five emitters. The transistor sizes were optimized to provide minimum noise in the oscillator. This was done with the noise summary feature in Cadence by minimizing the noise contribution of the transistors with regards to all other components in the circuit. Q_{CB} consists of 18 parallel-connected transistors, while Q_{CC} and Q_{OB} are 12 parallel-connected transistors. The total phase noise performance of the circuit was observed periodically while doing the optimization.

The inductors in the utilized BiCMOS process can be sized quite freely. The inductors in both the parallel and series resonance tanks were sized so that their quality factor would be good at the desired oscillation frequency. The small inductances 1.35 nH and 1.4 nH also result in physically smaller inductors, thus saving silicon area. The varactor was chosen to have quite high maximum capacitance (7.6 pF), since the series inductor is fairly small in terms of inductance. An NMOS-varactor provides a larger capacitance range than a PN-varactor with the available range of tuning voltages, and thus became the desired choice. The capacitors in both the parallel resonance tank and between transistor stages were realized as multiple small parallel-connected MIM-capacitors. For example capacitor C_P is made with four 325-fF capacitors connected in parallel. This was done in order to preserve the high *Q*-factor of the capacitor even when the capacitance must be larger, since a high *Q*-factor of both resonance tanks contributes to good phase noise performance.

When looking at the two resonance tanks in the schematic, it can be noticed that their center frequencies would be very different. However, it must be kept in mind that many parasitic capacitances are coupled to the parallel resonance tank, and that the nominal value given for the varactor is its maximum capacitance. With this in mind, the two resonance frequencies are a bit closer to each other than it may at first seem.

The bias resistors in the circuit were made as multiple parallel-connected resistors of equal size. For example, R_3 consists of four parallel-connected resistors of 360 Ω each. In this way the effects of process variations on the final real size of each resistor could be minimized. It also ensures that transistor bias currents will be close to the simulated currents, as long as there is nothing severely wrong with the transistors themselves. The resistor sizes were optimized so that the bias current through each transistor would be good with respect to its size and the noise produced in the transistor. This is another factor that affects the phase noise performance of the circuit. The noise summary feature of Cadence was again very helpful in minimizing the noise generated in the resistors and in the transistors through proper biasing.

The tuning range was made as large as possible by tuning the sizes of the varactor and the inductor in the series resonance feedback. The bias resistors and the bias current of the common-base transistor were also tuned in order to achieve a larger variation of the voltage at the emitter of the common-base stage. The large variation ensures that a greater part of the capacitance-voltage curve of the varactor is utilized, resulting in a greater tuning range.

4.2 Simulation results

The electrical performance of the circuit was simulated before sending the circuit to fabrication. Results from these simulations were used to optimize the values of the components in the circuit. Of main interest was to minimize phase noise and to maximize the frequency tuning range of the circuit. Figure 4.2 shows results from the phase noise and frequency tuning simulations.

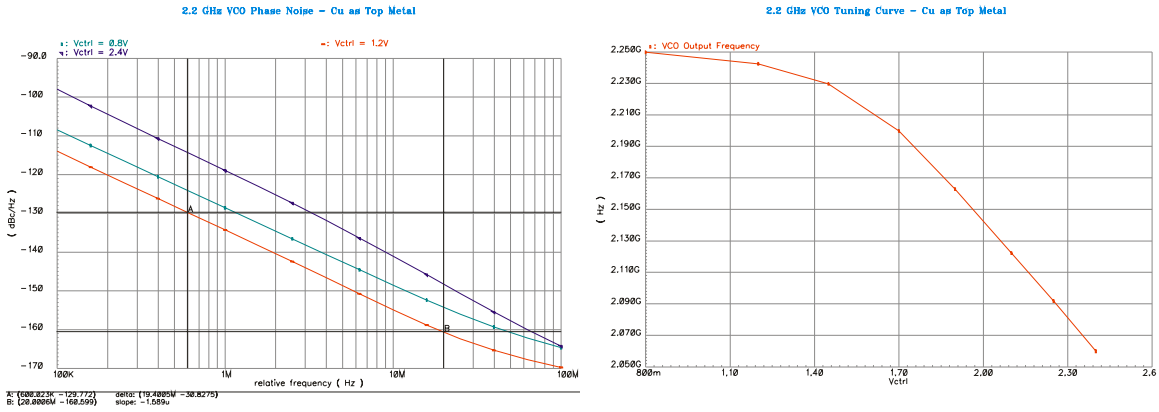

Figure 4.2. LC VCO simulated phase noise with three different control voltage values (left) and frequency tuning (right).

From these simulations it can be seen that the phase noise of the VCO changes quite heavily with the control voltage. This is mainly due to the changing noise properties of the common-base amplifier. In any case, the best phase noise performance of -144 dBc/Hz at an offset of 3 MHz is satisfactory. The simulation of frequency tuning shows that the tuning range is about 190 MHz. This is enough to cover for example the WCDMA band from 2.11 GHz to 2.17 GHz.

4.3 Circuit layout

The physical implementation of the LC VCO was done with Cadence Virtuoso, using parameterized cells (pcells) available in the design kit. Dummy transistors were added around the transistor arrays in order to avoid process variations on the outermost transistors, and the same was done for resistors. Mentor Calibre software was used for design rule checks (DRC) and layout vs. schematic (LVS) checking.

Part of the circuits were fabricated with copper as the top metal layer (Metal5), while others were fabricated with aluminum as the Metal5 layer. The layout was drawn with only aluminum Metal5, and the change to copper was made automatically during chip fabrication.

The general layout of the LC VCO is shown in Figure 4.3, with a more detailed picture of the core and its components in Figure 4.4. The micrograph of the fabricated chip is shown in Figure 4.5.

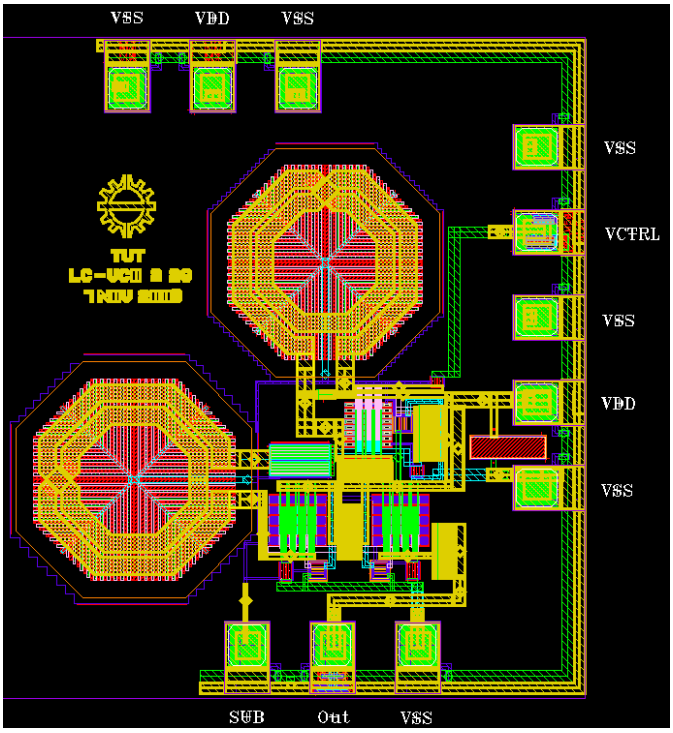

Figure 4.3. Layout of the LC VCO.

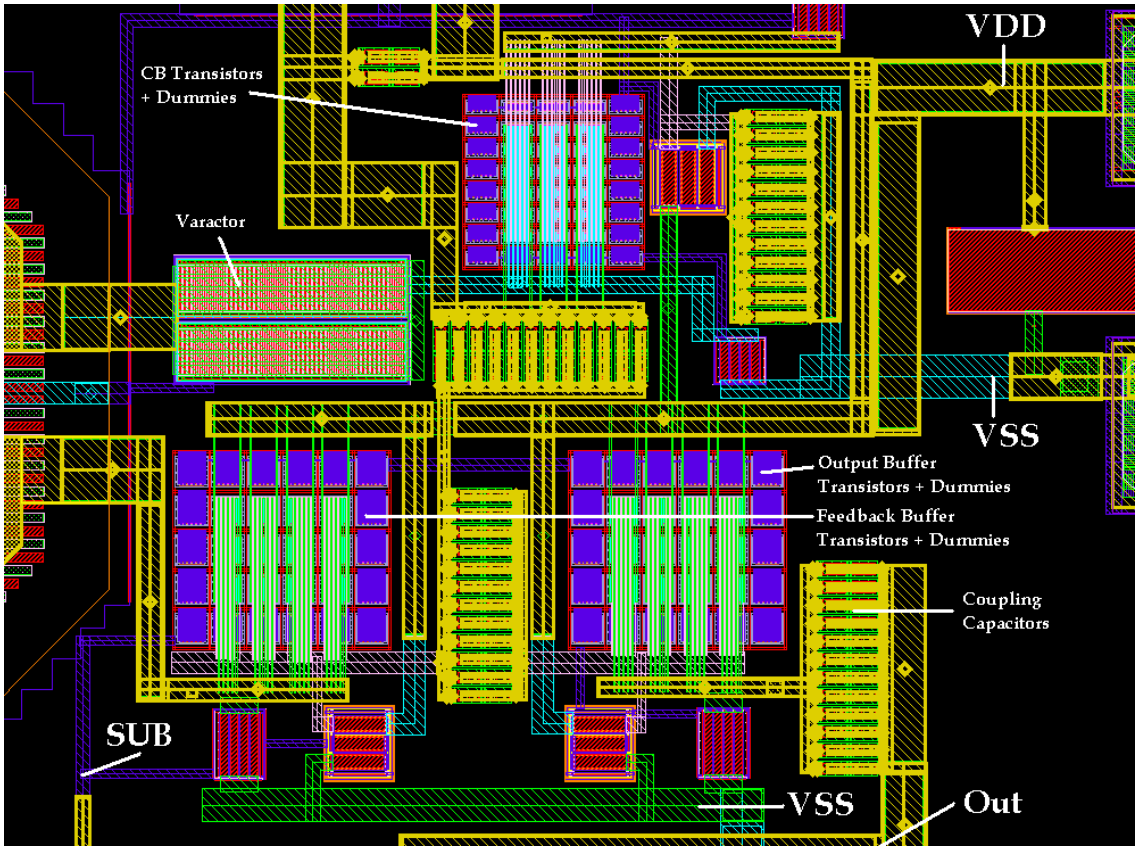

Figure 4.4. Detailed view of the LC VCO core layout.

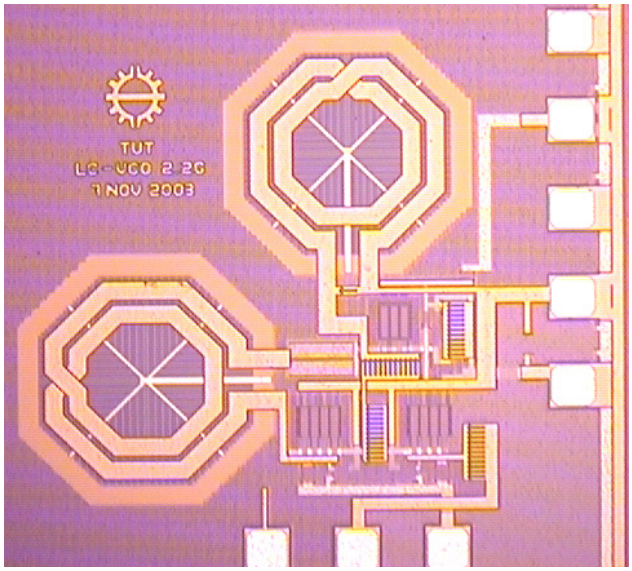

Figure 4.5. LC VCO chip micrograph.

4.4 Measurements

Measurements of the LC VCO were performed on single dies glued onto an Al_2O_3 (alumina) substrate. They were fed by a 2.4-V supply, and the output signal was connected to an HP4352S signal source analyzer or an R&S FSEM 26.5-GHz spectrum analyzer, depending on the measurement to be performed. A diagram summarizing the measurement setup is shown in Figure 4.6.

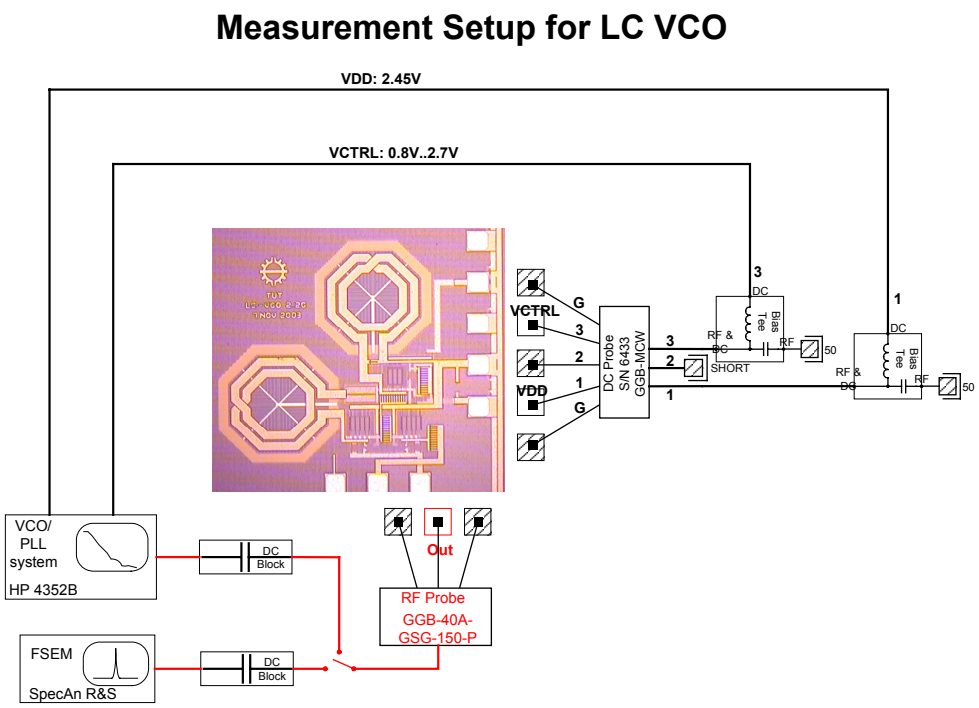

Figure 4.6. Measurement diagram for the LC VCO.

Figure 4.7 shows the output spectrum of the LC VCO. The picture on the left shows the spectral content close to the carrier. It can be seen that the spectrum around the carrier signal is quite pure, with no spurious signals appearing close to it. A wider picture of the spectrum is shown on the right. The second harmonic is attenuated by approximately 14 dB compared to the carrier.

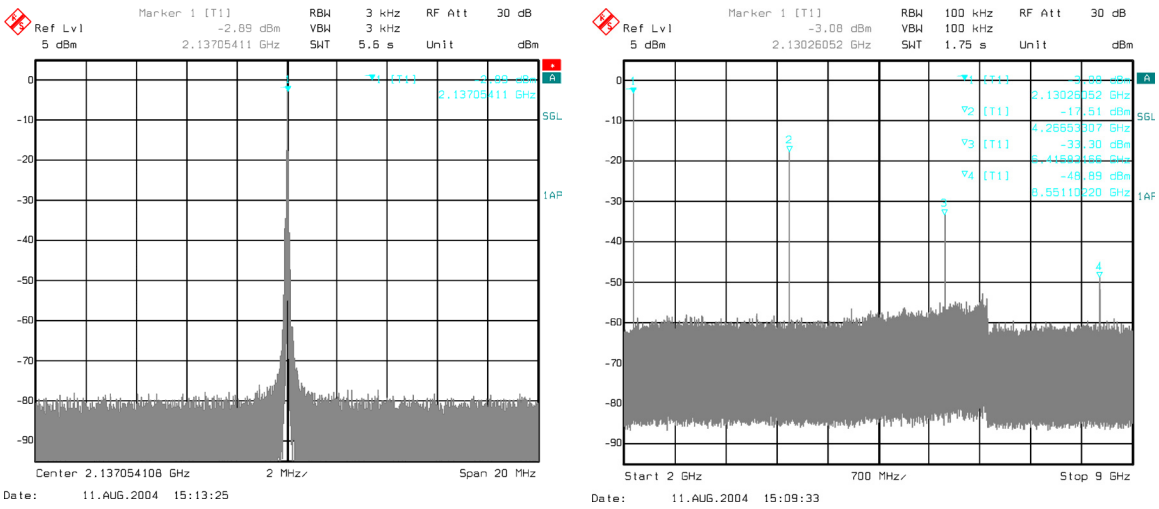

Figure 4.7. LC VCO output spectrum, only carrier (left) and carrier with harmonics (right).

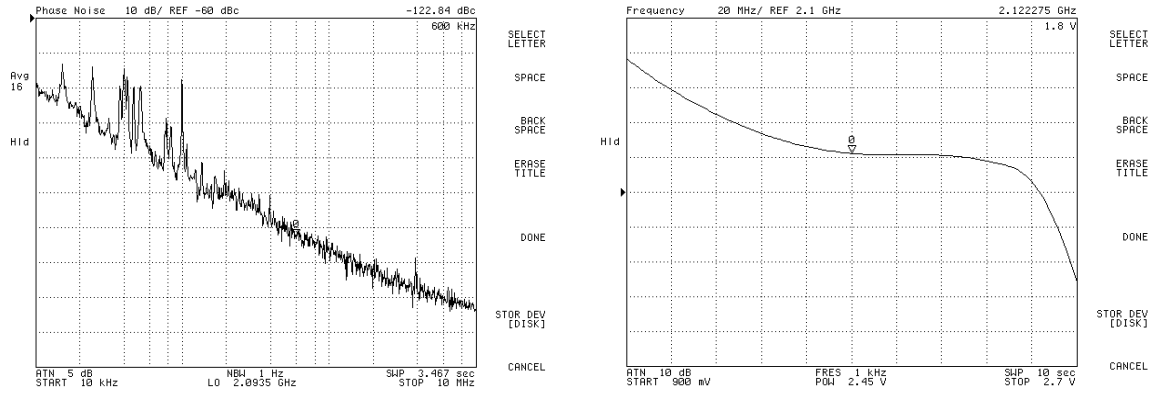

Figure 4.8. LC VCO measured phase noise (left) and frequency tuning (right).

Figure 4.8 shows the best phase noise performance and the frequency tuning performance of the LC VCO. The best phase noise is -135.0 dBc/Hz at an offset of 3 MHz from the carrier. This value is approximately 9 dB worse than what was simulated. The reason for this difference is not entirely clear, although insufficient modeling of circuit parasitics in the form of line resistances is suspected to be one reason. Variations of resonance tank component values based on fabrication tolerances may be another reason.

The tuning range of 128 MHz is also not as good as the simulated one. In addition, it is received by extending the tuning voltage range up to 2.7 V instead of the 2.4 V used in simulations. It was not possible to use control voltage values below 0.9 V, because the common-base amplifier is then shut down and oscillation ceases. In any case, the achieved tuning range is enough to cover for example one 60-MHz-wide WCDMA band.

As was predicted during the electrical simulations, the phase noise of the LC oscillator was not constant throughout the frequency tuning range. The phase noise at a 3-MHz offset from the carrier is shown in Figure 4.9 for the whole tuning range in order to illustrate the fluctuation of the phase noise as a function of the control voltage. The total variation is about 9 dB.

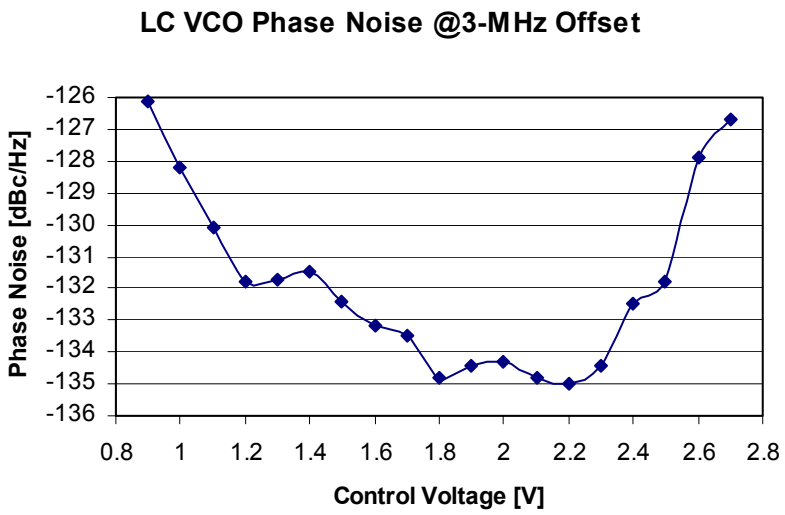

Figure 4.9. LC VCO measured phase noise at a 3-MHz offset as a function of the control voltage.

The measured output power and frequency pushing of the VCO are shown in Figure 4.10. The maximum output power is about -1.5 dBm, which is sufficient for good measurement precision. It can also be seen that the output power of the circuit varies significantly throughout the control voltage range. This is mainly due to the changing gain of the common-base amplifier. Frequency pushing performance is seen on the right, and the pushing figure of this VCO is 25 MHz/V.

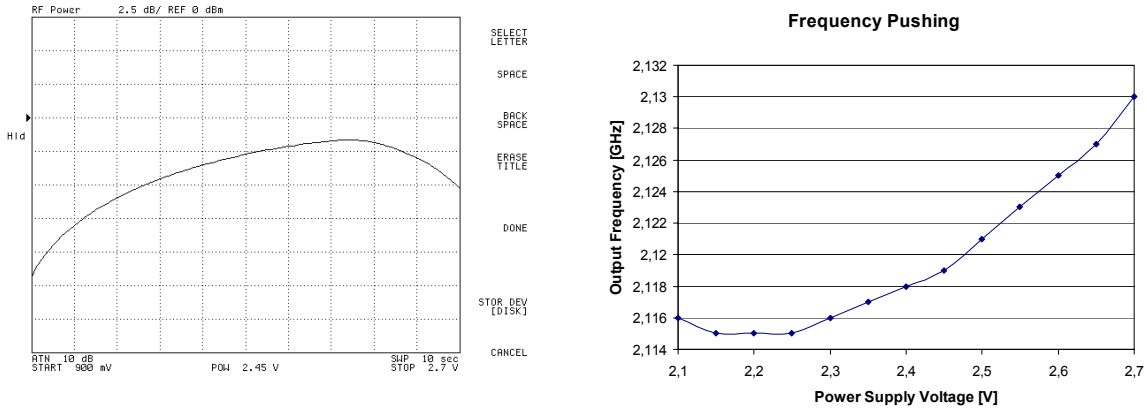

Figure 4.10. LC VCO output power vs. control voltage (left) and frequency pushing with V_{CTRL} = 1.7 V (right).

A summary of the simulation and measurement results of this reference LC VCO is given in Table 4.1.

Table 4.1. Summary of LC VCO simulation and measurement results, V_{CC} = 2.4 V.

Parameter	Simulated	Measured	Unit
Current consumption	11 - 25	11 - 26	mA
Tuning range	190	60 (128)*	MHz
f_{min}	2.06	2.12 (2.05)*	GHz
f_{max}	2.25	2.18	GHz
Phase noise @3 MHz			
Best	-144.0	-135.0	dBc/Hz
Worst	-129.0	-126.1	dBc/Hz
Output power	-	-12 … -1.7	dBm
Pushing figure	-	25	MHz/V

* With control voltage extended from 2.4 V to 2.7 V.

All in all it can be said that the VCO works, although there are differences between the simulations and the measurements. The differences may partly be due to fabrication tolerance variations and insufficient modeling of circuit parasitics. Despite these differences, the LC VCO is a good testbench for later comparisons with the FBAR VCO.

5 A 2.1-GHz Above-IC-FBAR VCO in 0.25-µm SiGe BiCMOS

This chapter describes the design and measurements of two versions of an above-IC-FBAR VCO for the 2.1-GHz frequency area. Both oscillator cores have the same structure, but one of the oscillators has a single-ended output, while the other one has a differential output. The oscillators were simulated with Cadence IC 5.0 and Spectre, the layout was done with Cadence Virtuoso, and the DRC and LVS checks were performed using Mentor Calibre software. Layout parasitics were manually estimated and included in the electrical simulations.

The circuits were fabricated in a 0.25-µm SiGe BiCMOS technology of ST Microelectronics, with the FBAR built on top of the IC through post-processing steps performed by CEA-LETI and CSEM. Due to some problems in the post-processing, the protection layer above the contact pads was at first intact and had to be removed. The removal process at CSEM was successful, and it then became possible to measure the circuits. The circuits were sent for fabrication in September 2004, and measurements became possible in June 2005.

5.1 Schematic diagram

Figure 5.1 shows the schematic diagram of the single-ended version of the FBAR VCO. The only notable difference to the single-ended LC VCO presented in chapter 4 is the replacement of the series resonance LC tank by the FBAR. Some changes in the values

of components R_3 and L_p were also done in order to optimize the performance of the circuit. Thus the differences between the LC VCO and the FBAR VCO are very small, and a fair comparison between the performances of the two can be made later.

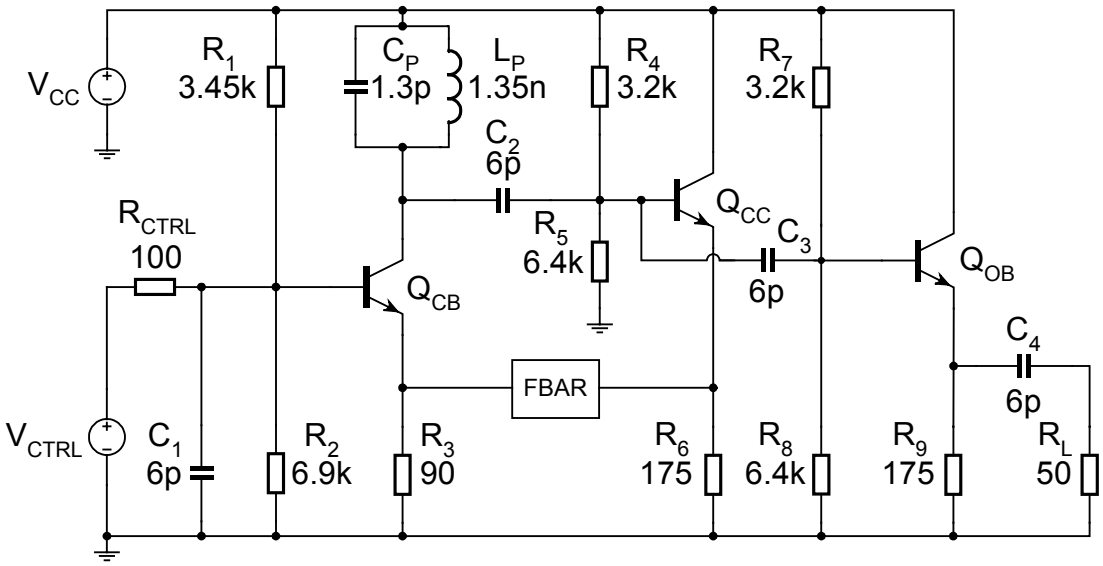

Figure 5.1. Schematic of the single-ended 2.1-GHz FBAR VCO.

A differential-output version of the FBAR VCO was also designed, seen in Figure 5.2. The core of that oscillator is nearly identical to the single-ended FBAR VCO (there is a small difference in the parallel LC tank), but the common-collector output buffer is replaced by the more complex buffering system described in subchapter 3.4. Capacitor C_4 has been added in order to decrease the large amplitude of the signal entering the differential amplifier transistor Q_{D1}, thus preventing the differential amplifier from saturating. This differential-output version of the VCO was also successfully integrated at ST Microelectronics with an experimental receiver, with a mixer serving as the differential load impedance of the oscillator. However, an analysis of that situation is beyond the scope of this thesis.

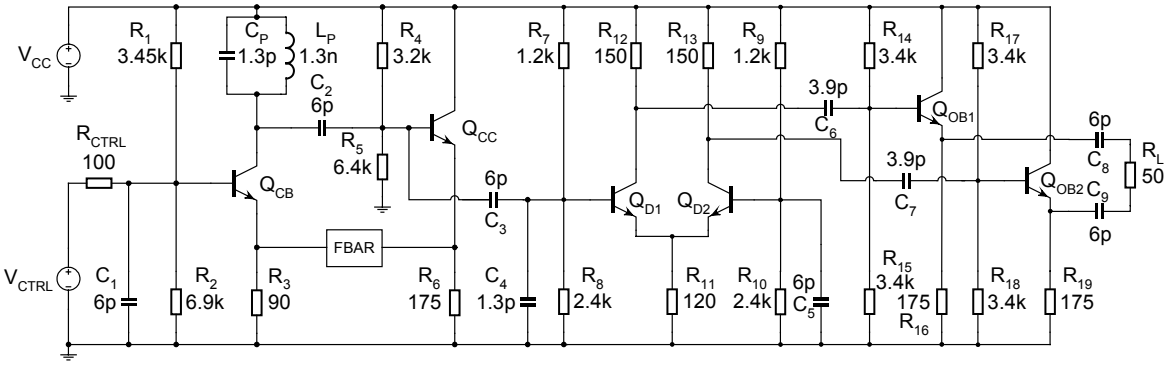

Figure 5.2. Schematic of the differential-output 2.1-GHz FBAR VCO.

The FBAR was included as a lumped-element model (Figure 5.3) during circuit simulations. The series resonance frequency of the model is 2.15 GHz, and its series resonance *Q*-factor is 512. The physical footprint size of the actual device including the electrodes is about 0.11 mm^2.

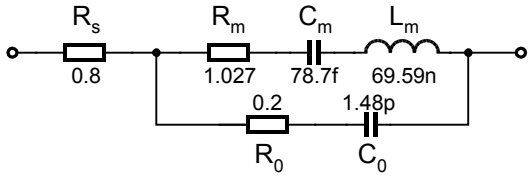

Figure 5.3. MBVD model of the 2.15-GHz FBAR.

5.2 Simulation results

The electrical simulations were done by using the Spectre simulator in Cadence. As with the LC oscillator, the most interesting properties were again phase noise and frequency tuning performance. Simulations of these two properties are in Figure 5.4 and Figure 5.5 for the single-ended version, with the same results for the differential-output version being shown in Figure 5.6 and Figure 5.7.

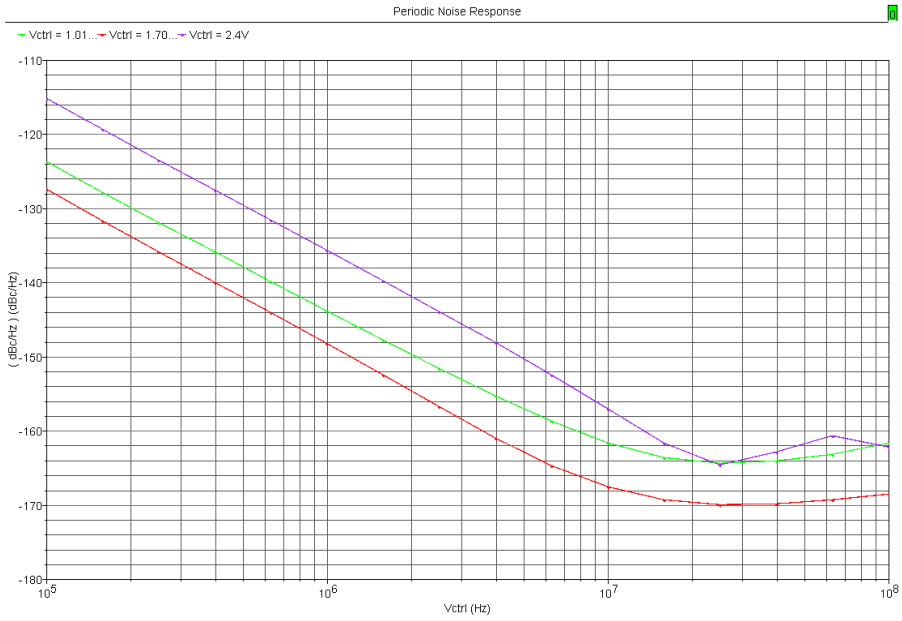

Figure 5.4. Single-ended FBAR VCO simulated phase noise with three control voltage values.

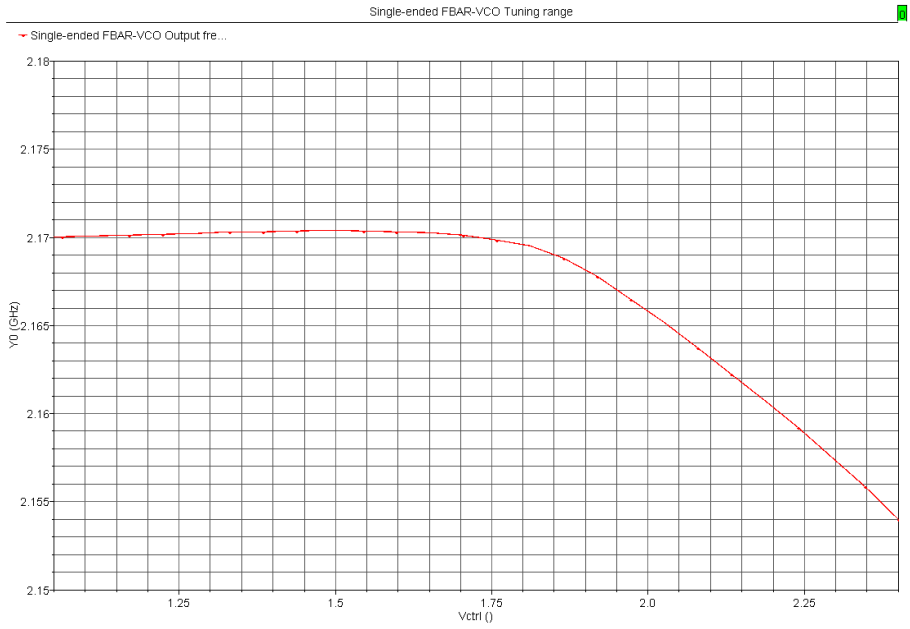

Figure 5.5. Single-ended FBAR VCO simulated frequency tuning.

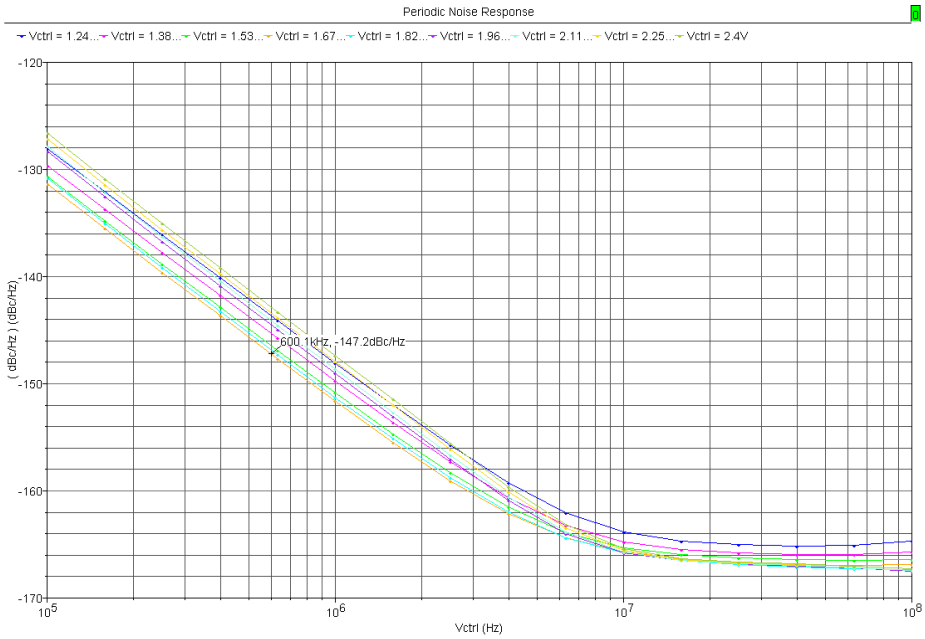

Figure 5.6. Differential-output FBAR VCO simulated phase noise with a few control voltage values.

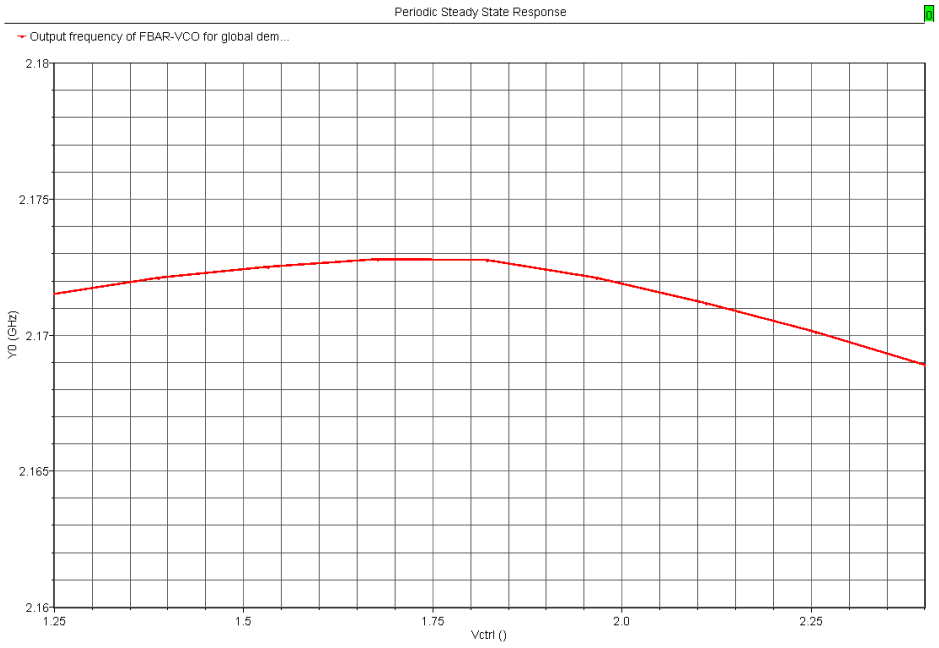

Figure 5.7. Differential-output FBAR VCO simulated frequency tuning.

The simulations show very good phase noise performance at the optimum tuning voltage. At a 3-MHz offset the best phase noise is -158.3 dBc/Hz for the single-ended version and -160.2 dBc/Hz for the differential-output version of the oscillator. The

benefits to phase noise of using a high-*Q* resonator are thus clearly seen. The phase noise varies depending on control voltage, as was expected and also seen in the LC oscillator.

The second prediction concerning the effect of a high quality factor on oscillator performance is also evident in the simulations. This is the reduced frequency tuning range, with the available tuning being 16 MHz for the single-ended version and a mere 4 MHz for the differential-output circuit. In any case this is encouraging, considering the achieved frequency tuning in earlier FBAR oscillator implementations.

5.3 Circuit layout

The layout of the FBAR VCO circuit used as its basis the layout of the LC VCO. Some minor changes were made, most notable of which was the removal of the series resonance LC tank. Signal wires for the FBAR were drawn, but the footprint of the FBAR itself was added during later steps that were not under my control. Another notable change was the removal of dummy transistors. This was done because they introduced a lot of parasitic resistance by lengthening critical signal paths. Pictures of the two layouts are in Figure 5.8.

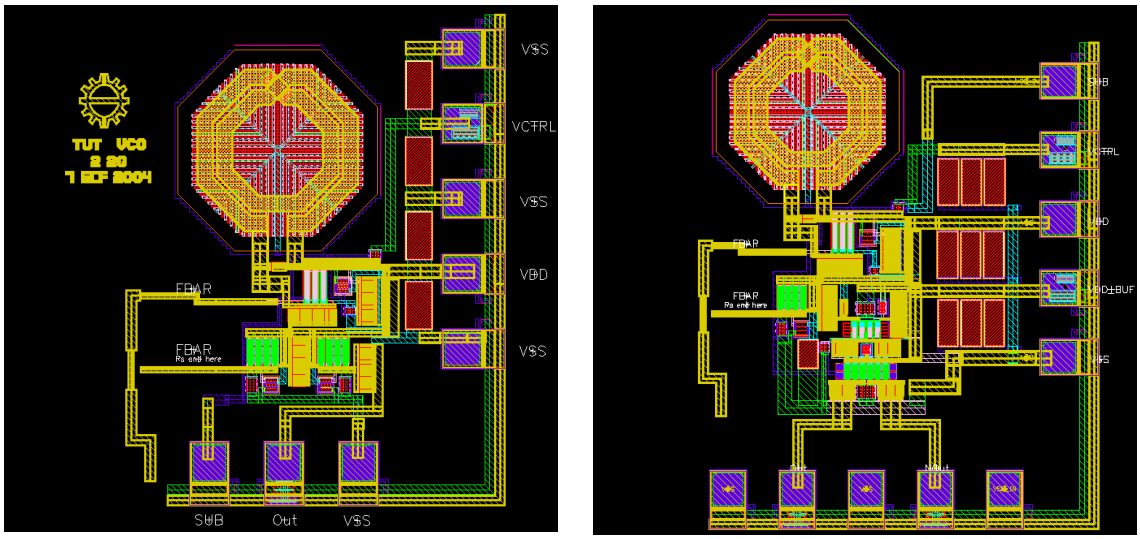

Figure 5.8. Layout of the single-ended (left) and differential-output (right) FBAR VCOs.

It will be noticed that the differential-output version has two more pads compared to the single-ended version. They have been added in order to realize the differential output. The differential-output version also has more capacitors that filter the power supply and control voltage DC lines. In addition, the differential-output version

contains a separate power supply line for the buffers. The micrographs of the fabricated circuits including the FBAR devices are shown in Figure 5.9.

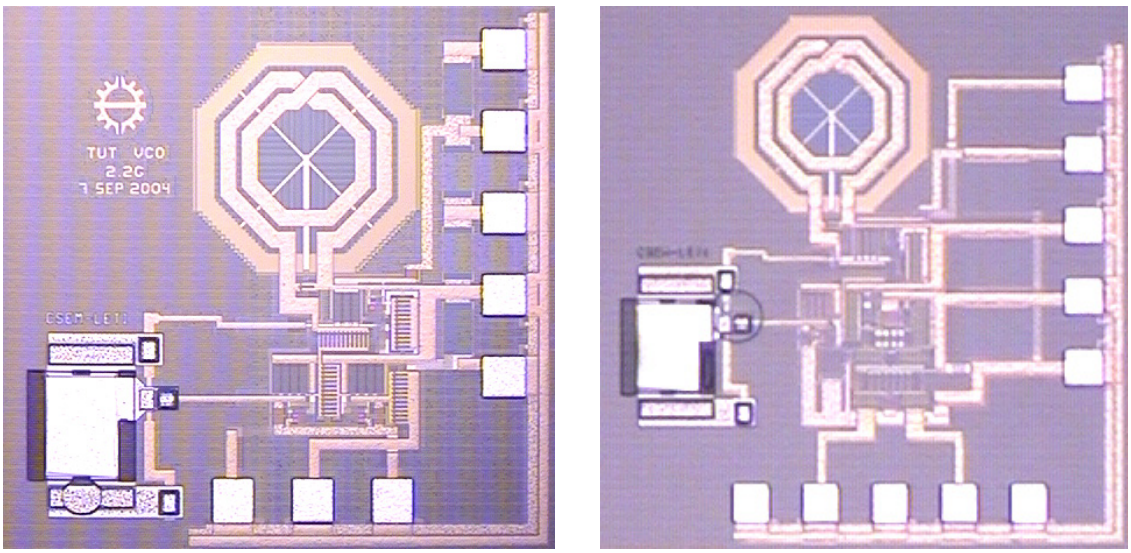

Figure 5.9. FBAR VCO chip micrographs, single-ended (left) and differential-output (right) versions.

5.4 Measurements

The main difference between measuring the LC VCO and the FBAR VCO circuits is that the FBAR oscillators were part of a larger wafer, and it was therefore not necessary to glue the single dies onto a separate substrate. The same measurement setup was used for the single-ended FBAR VCO as the one detailed in subchapter 4.4, and it is shown in Figure 5.10.

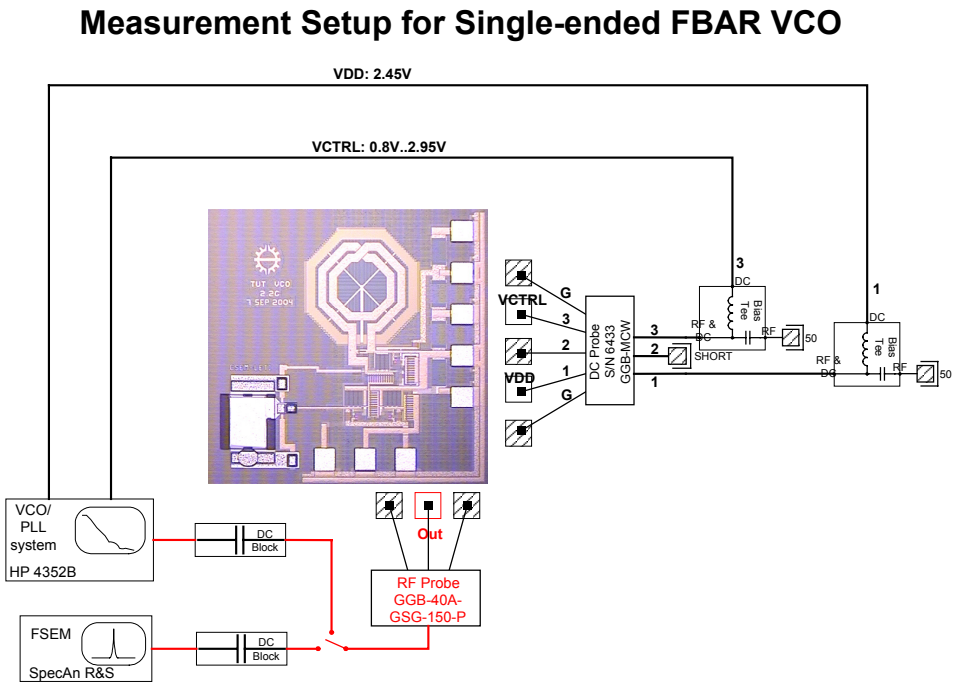

Figure 5.10. Measurement diagram for the single-ended FBAR VCO.

The differential-output FBAR VCO also uses the same setup, but it required a different type of probe at the output. One of the output signals was fed into the measurement instruments, and the other one was terminated with a 50-ohm connector. The full differential output power of the circuit was thus not used, but it was not necessary due to the satisfactory power level received already from one output. The measurement setup for the differential-output oscillator is shown in Figure 5.11.

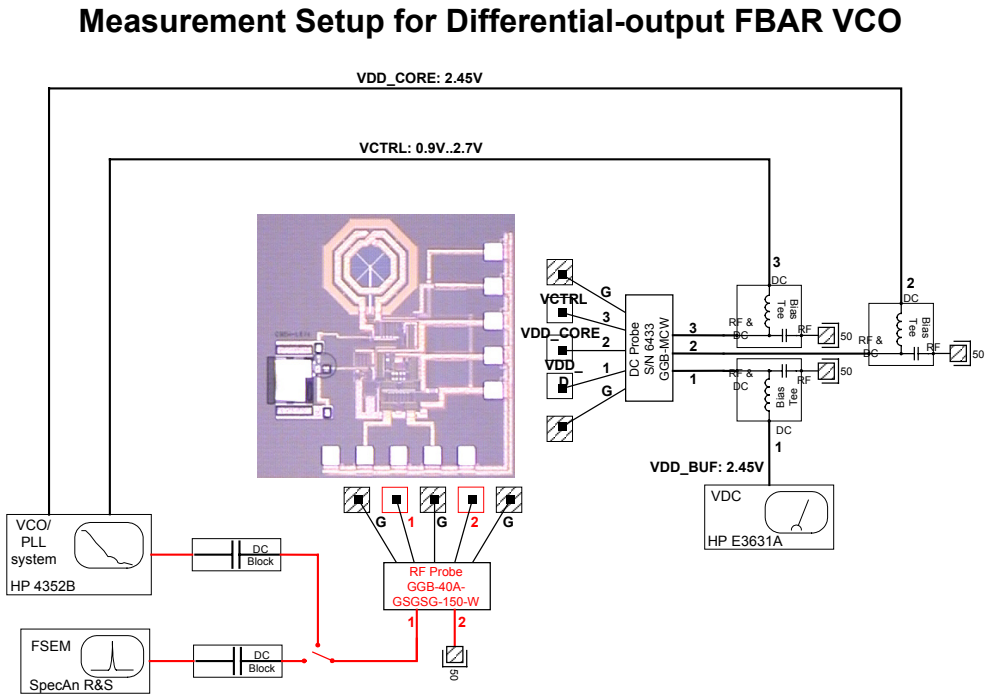

Figure 5.11. Measurement diagram for the differential-output FBAR VCO.

The output spectrum of the single-ended oscillator is shown in Figure 5.12. The spectrum is quite clean and shows no extra peaks next to the carrier. The second harmonic is attenuated by about 13.5 dB compared to the carrier.

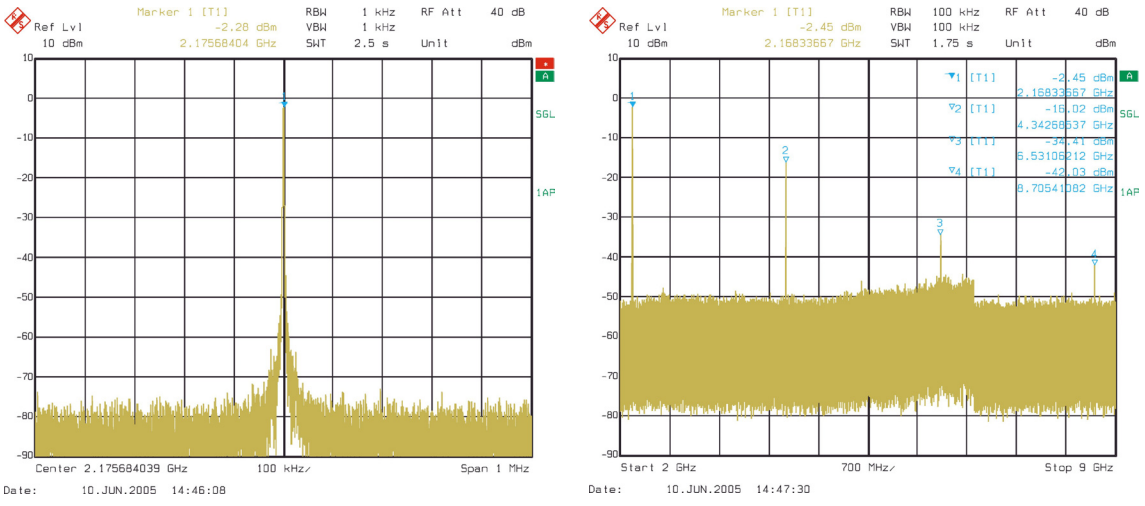

Figure 5.12. Single-ended FBAR VCO output spectrum, only carrier (left) and carrier with harmonics (right).

Figure 5.13 shows the best phase noise performance and the frequency tuning performance of the single-ended FBAR VCO. The phase noise is -149.6 dBc/Hz at an

offset of 3 MHz from the carrier, and the noise floor of approximately -150 dBc/Hz is reached at an offset of about 5 MHz. The total amount of available frequency tuning is about 37 MHz, with most of the tuning taking place at higher values of the control voltage. The lowest utilized control voltage was 0.9 V, because oscillations cease below that value. In order to find out the maximum tuning range, the control voltage was extended all the way up to 2.95 V. With another sample of the circuit it was noticed that the oscillator was not able to operate on all frequencies within the tuning range. This was seen by abrupt vertical jumps appearing in the tuning curve. The center frequency of that sample was about 70 MHz higher than that of the present sample. Therefore it is likely that the malfunctioning occurs due to the different conditions and mechanisms in the interplay between the parallel LC resonator and the resonance characteristics of the FBAR.

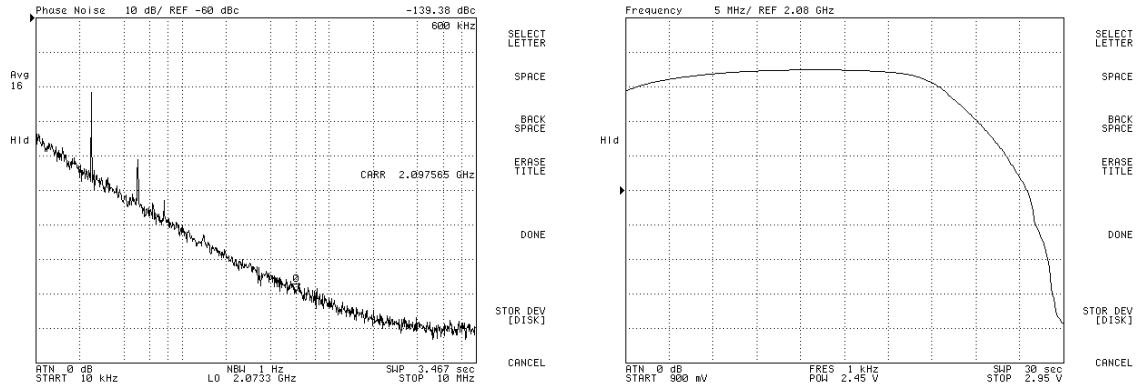

Figure 5.13. Single-ended FBAR VCO phase noise (left) and frequency tuning (right).

The output power and the frequency pushing performance of the single-ended circuit are shown in Figure 5.14. The maximum output power is about -2 dBm, and the variation throughout the tuning range is approximately 11 dB. This output power is sufficient for receiving reliable measurement results. The output frequency of the VCO changes about 3 MHz with a 0.6-V change in the power supply voltage, translating into a pushing figure of 5 MHz/V.

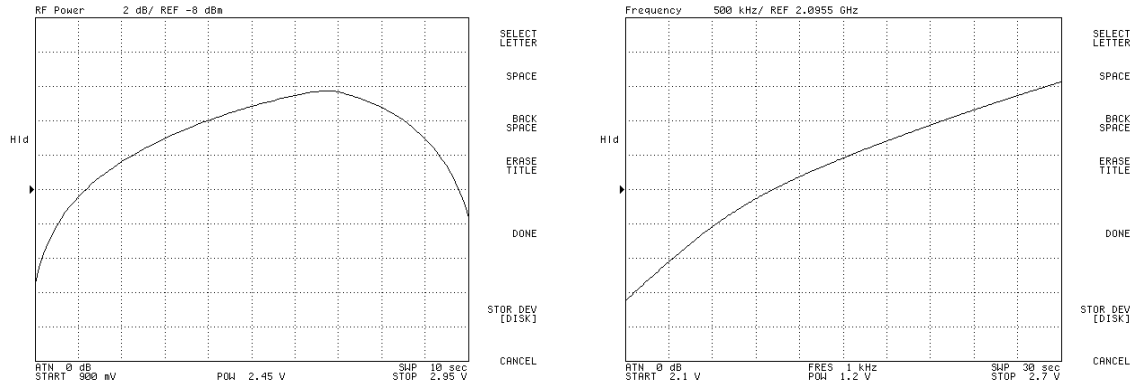

Figure 5.14. Single-ended FBAR VCO output power vs. control voltage (left) and frequency pushing (right).

Moving on to the differential-output FBAR VCO, its output spectrum pictures are seen in Figure 5.15. The spectrum is again clean and devoid of spurious signals, with the second harmonic being attenuated about 11.5 dB compared to the carrier.

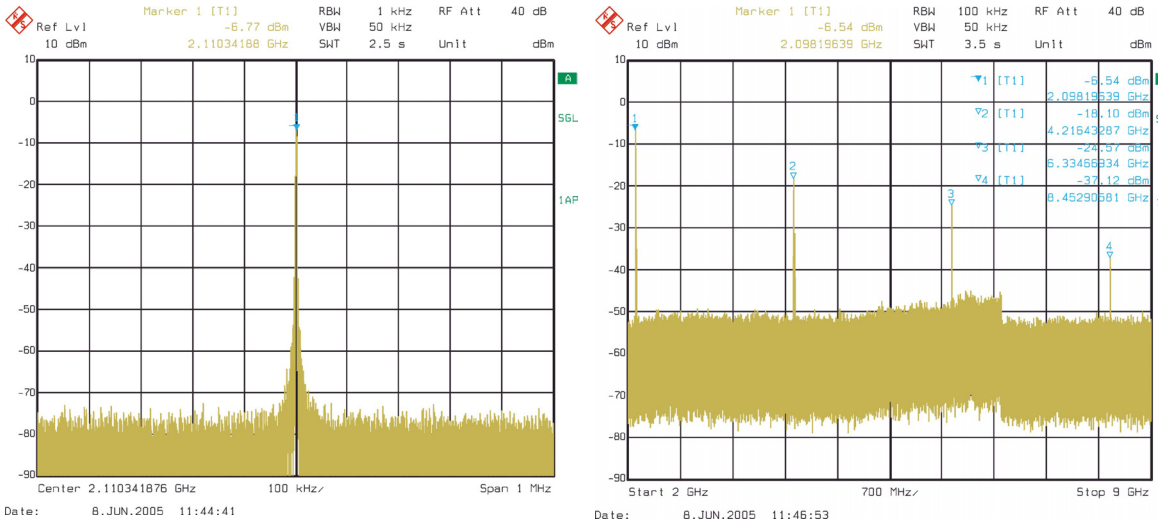

Figure 5.15. Differential-output FBAR VCO output spectrum, only carrier (left) and carrier with harmonics (right).

The phase noise and frequency tuning plots are shown in Figure 5.16. The phase noise is -147.3 dBc/Hz at a 3-MHz offset, and a phase noise floor of about -147 to -148 dBc/Hz is reached at an offset of between 2 and 3 MHz. The output frequency of the differential-output VCO can be tuned approximately 15 MHz when using 2.7 V as the maximum control voltage.

As with the single-ended VCO, the measurement of another sample of the circuit showed that there were some areas within the tuning range at which the circuit could not

oscillate. It was again seen by abrupt vertical jumps appearing in the tuning curve. This was not the case with the sample producing the measurement results in the figures below, however. The center frequency of the other sample was approximately 25 MHz higher, and it is possible that the interplay between the parallel LC resonator and the FBAR was not the same as in the present sample.

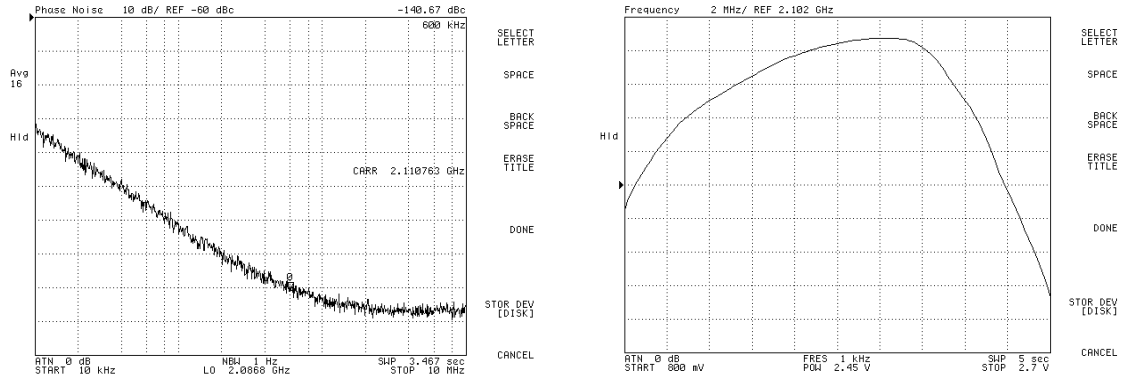

Figure 5.16. Differential-output FBAR VCO phase noise (left) and frequency tuning (right).

The single-ended output power and the pushing figure of the differential-output oscillator are shown in Figure 5.17. The power of the output signal is about -8 dBm and shows no significant changes throughout the tuning range. The pushing figure of the differential-output FBAR VCO is approximately 5 MHz/V, which is the same as that of the single-ended version.

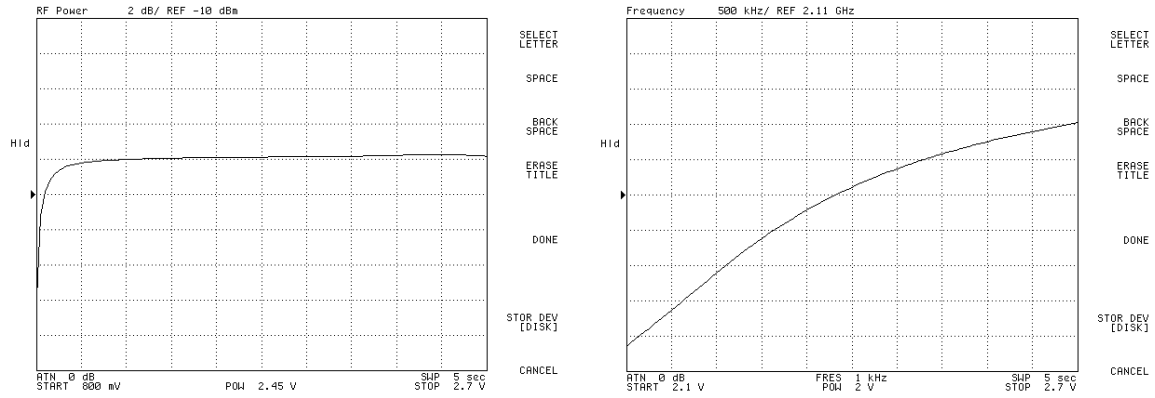

Figure 5.17. Differential-output FBAR VCO output power vs. control voltage (left) and frequency pushing (right).

Since the phase noise of the single-ended and differential-output VCO versions both change with control voltage, it is of interest to see where and to what extent these changes appear. A plot illustrating the phase noise is shown in Figure 5.18.

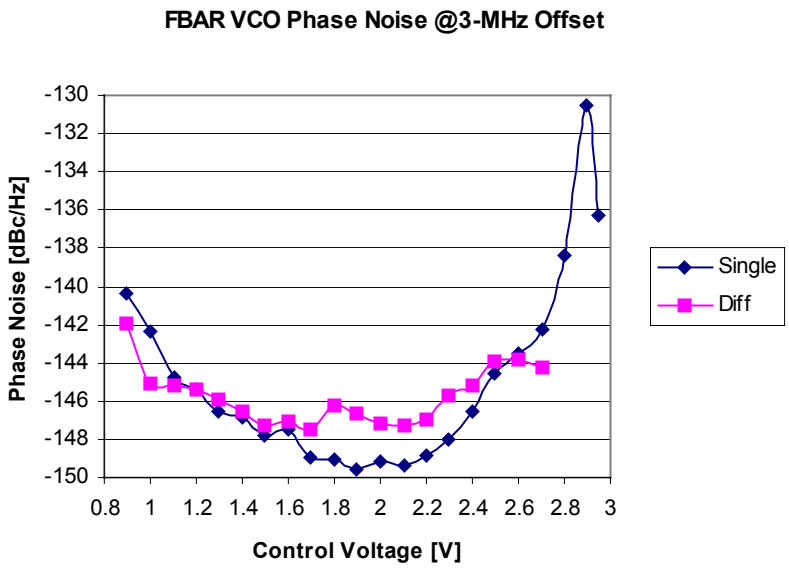

Figure 5.18. The phase noise of the single-ended and differential-output FBAR VCOs at a 3-MHz offset as a function of control voltage.

The simulated and measured performance metrics of the FBAR VCO versions are collected together in Table 5.1.

Table 5.1. Summary of FBAR VCO simulation and measurement results, V_{CC} = 2.4 V.

	Single-ended		**Differential-output**		
Parameter	**Simulated**	**Measured**	**Simulated**	**Measured**	**Unit**
Current consumption	-	11 – 29	-	22 – 39	mA
Tuning range	16*	37	4*	15	MHz
f_{min}	2.154	2.061	2.169	2.096	GHz
f_{max}	2.170	2.098	2.173	2.111	GHz
Phase noise @3 MHz					
Best	-158.3	-149.6	-160.2	-147.3	dBc/Hz
Worst	-145.7	-130.6	-157.0	-141.9	dBc/Hz
Output power	-	-13 … -2.5	-	-15 … -6.5	dBm
Pushing figure	-	5	-	5	MHz/V

* These numbers refer to simulations where the maximum value of V_{CTRL} was 2.4 V. In the measurements, maximum tuning voltages of 2.95 V and 2.7 V were used for the single-ended and differential-output VCOs, respectively.

Both FBAR VCO circuits are functional and have reasonably large tuning ranges. This is encouraging, considering how difficult it has traditionally been to design frequency-tunable high-*Q* oscillators. The measured phase noise is between 9 and 15 dB higher than the simulated phase noise. A noise floor appears in both VCOs close to -150 dBc/Hz, with the floor of the differential-output version being a bit higher partly due to the complex output buffering. A lowering of the floor can be noticed when increasing the power supply voltage of the buffering section of the differential-output oscillator. Both VCOs also operate close to the noise floor of the measurement system, so that may have an effect on the placement of the noise floor.

Although the measured phase noise does not quite live up to the simulated performance, it is still very good and indicates high frequency stability. The frequency tuning of the oscillators is satisfactory, but as mentioned earlier, it comes at the cost of changing phase noise. While keeping this tradeoff in mind, however, the frequency tuning performance is very encouraging. Compared with earlier FBAR oscillators, the frequency tuning is very good and the highest yet reported.

6 LC VCO and FBAR VCO Comparison

The LC oscillator and both FBAR oscillators are functional, and although their measured performance deviates from the simulations, they work in a satisfactory manner. A comparison of the measurement results is given in Table 6.1.

Table 6.1. Comparison of FBAR VCO and LC VCO measured performance.

Parameter	Single-ended FBAR VCO	Diff-output FBAR VCO	Reference LC VCO	Unit
Current consumption	11 - 30	22 - 39	11 - 26	mA
Tuning range	37	15	128	MHz
f_{min}	2.061	2.096	2.05	GHz
f_{max}	2.098	2.111	2.18	GHz
Phase noise @3 MHz				
Best	-149.6	-147.3	-135.0	dBc/Hz
Worst	-130.6	-141.9	-126.1	dBc/Hz
Output power	-13 ... -2.5	-15 ... -6.5	-12 ... -1.7	dBm
Pushing figure	5	5	25	MHz/V
FOM	-193	-192	-177	dB

The frequency tuning performance follows the expectations as far as comparative tuning range magnitude between the oscillator versions goes. The oscillation frequency of

the FBAR oscillators is lower than simulated, however. This is most likely due to a different resonance frequency of the FBAR devices in the particular circuits that were measured. Because the FBAR has a very high *Q*-factor, it is the component most critical in determining oscillation frequency. It would therefore be very important to have its resonance frequency more stably determined throughout the wafer and the fabrication process, if mass production is a desirable goal. The tuning range of the FBAR VCO was larger than simulated, which is encouraging when thinking of future developments. It is still noticeably smaller than the tuning range of the LC oscillator.

The phase noise of both FBAR VCO versions is clearly superior compared to that of the LC VCO, as was predicted both in the theoretical considerations and in the electrical simulations. This is true at both low and high offsets. When varying the control voltage, the phase noise of all VCO versions changes. An instructive plot comparing the LC VCO and FBAR VCO phase noise at a 3-MHz offset throughout their tuning ranges is given in Figure 6.1.

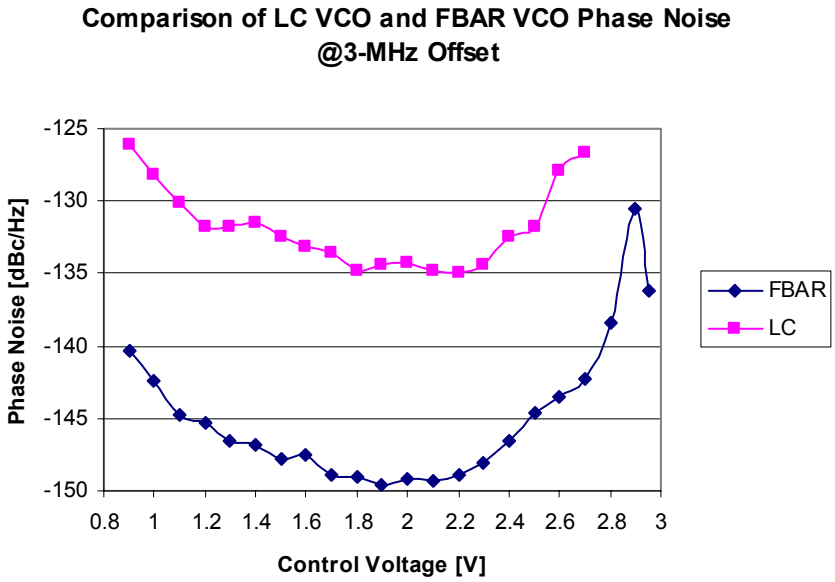

Figure 6.1. Comparison of LC VCO and single-ended FBAR VCO phase noise throughout the control voltage range.

The best-case phase noise of the LC VCO is about 5 dB better than the worst-case phase noise of the FBAR VCO at a 3-MHz offset. However, keeping in mind that the phase noise is non-constant in all VCO versions, the FBAR VCO can in general be said to perform considerably better than the LC VCO in terms of phase noise. To get a feel for the best phase noise performance of the oscillators, the sweet-spot phase noises are

compared in Figure 6.2. It can be seen that before the FBAR oscillator reaches its noise floor, its phase noise is approximately 15 dB better than that of the LC oscillator.

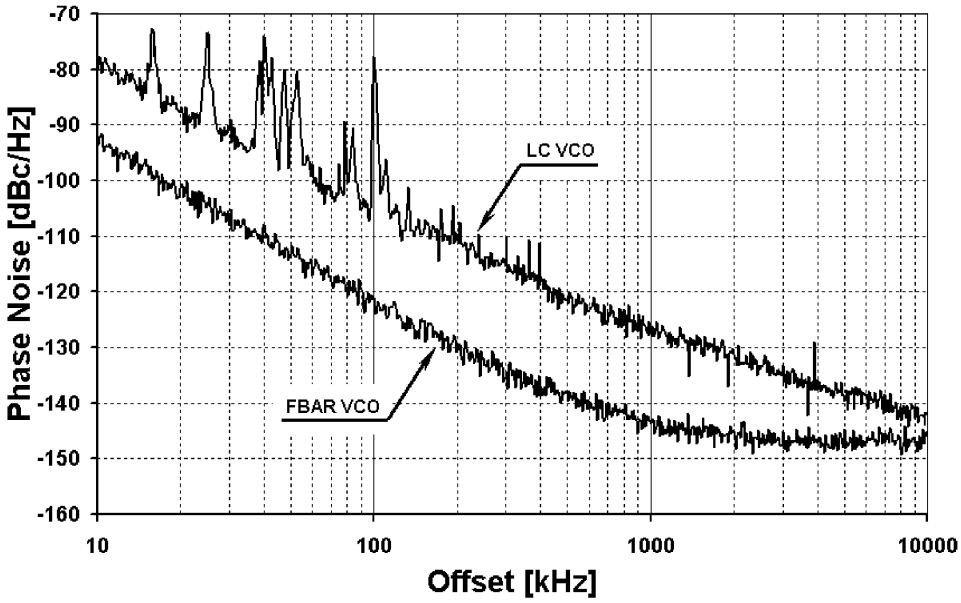

Figure 6.2. Comparison of best phase noises of the LC VCO and the differential-output FBAR VCO.

As a summary it can be said that both the FBAR and the LC approach have their pros and cons. When extremely low phase noise is required and tuning range is not a high priority, the FBAR approach provides very good performance. On the other hand, when one desires to use the VCO in applications where larger bandwidth is required, the LC approach yields satisfactory performance. The FOM given in Table 6.1 is calculated using the best phase noise at a 1-MHz offset and the power consumption that corresponds to the control voltage with which the best performance was obtained. It can be seen that the FOMs of the FBAR oscillators are considerably better than that of the LC oscillator, but as explained in this paragraph, it is not the whole truth and does not take everything into account. Compared with earlier FBAR oscillator implementations, the present FBAR VCOs suffer from rather high power consumption, and therefore the FOM is not as good as it could be.

7 Conclusions

Integrating high-*Q* devices and implementing frequency tuning in oscillators that utilize high-*Q* resonators have traditionally been difficult problems. Recently it has become possible to build FBARs on top of monolithic circuits, thus taking care of the problem of integratability to some degree. Frequency tuning solutions have been proposed earlier, but these have not been able to provide tuning sufficient for multi-channel applications.

The mechanism employed in the first above-IC-FBAR VCO herein presented overcomes some of the problems with tuning. The experimental 2.1-GHz single-ended oscillator achieved a best phase noise of -149.6 dBc/Hz at a 3-MHz offset from the carrier. The tuning range of the circuit is about 37 MHz, or 1.8 %. It is thus clear that the solution proposed for realizing a larger tuning range than previously with a narrow-band FBAR works.

The achieved frequency tuning range is considerably larger than for any FBAR oscillator previously reported, and although it is still comparatively small and comes at the cost of changing phase noise performance, it can be successfully exploited. The obtained results also suggest that FBAR oscillator circuits with reasonably large frequency tuning ranges can successfully be made.

The most important future developments would be to capitalize on the possibility for decreased power consumption in FBAR oscillators and especially to find out how to best tune the FBAR without causing damage to its quality factor and thus the phase noise of the oscillator. Attaining these goals will require significant further research and development in order to find the most suitable circuit architectures and techniques.

References

[1] M.-A. Dubois, C. Billard, C. Muller, G. Parat, and P. Vincent, "Integration of High-Q BAW Resonators and Filters Above IC," *IEEE Int. Solid-State Circuits Conf. Dig. Tech. Papers*, Feb. 2005, pp. 392-393, 606.

[2] P.-H. Sung, C.-M. Fang, P.-Z. Chang, Y.-C. Chin, and P.-Y. Chen, "The Method for Integrating FBAR with Circuitry on CMOS Chip," *Proc. IEEE 2004 Int. Frequency Control Symposium and Exposition*, pp. 562-565.

[3] J.F. Carpentier, A. Cathelin, C. Tilhac, P. Garcia, P. Persechini, P. Conti, P. Ancey, G. Bouche, G. Caruyer, D. Belot, C. Arnaud, C. Billard, G. Parat, J.B. David, P. Vincent, M.A. Dubois, and C. Enz, "A SiGe:C BiCMOS WCDMA Zero-IF RF Front-End Using an Above-IC BAW Filter," *IEEE Int. Solid-State Circuits Conf. Dig. Tech. Papers*, Feb. 2005, pp. 394-395.

[4] R. Aigner, "High Performance RF-Filters Suitable for Above IC Integration: Film Bulk-Acoustic-Resonators (FBAR) on Silicon," *Proc. IEEE 2003 Custom Integrated Circuits Conference*, pp. 141-146.

[5] A.R. Hambley, *Electronics*, 2nd ed., Prentice Hall, 2000, pp. 636-640.

[6] J.-M. Mourant, J. Imbornone, and T. Tewksbury, "A Low Phase Noise Monolithic VCO in SiGe BiCMOS," *IEEE 2000 RFIC Symposium Digest of Papers*, pp. 65-68.

[7] R.B. Staszewski, C.-M. Hung, D. Leipold, and P.T. Balsara, "A First Multigigahertz Digitally Controlled Oscillator for Wireless Applications," *IEEE Transactions on Microwave Theory and Techniques*, vol. 51, no. 11, November 2003, pp. 2154-2164.

[8] Thomas H. Lee, *The Design of CMOS Radio-Frequency Integrated Circuits*, Cambridge University Press, 1998, pp. 532-536.

[9] R.C. Ruby, P. Bradley, Y. Oshmyansky, A. Chien, and J.D. Larson III, "Thin Film Bulk Acoustic Resonators (FBAR) for Wireless Applications," *Proc. IEEE 2001 Ultrasonics Symposium*, vol. 1, pp. 813-821.

[10] M. Ylilammi, J. Ellä, M. Partanen, and J. Kaitila, "Thin Film Bulk Acoustic Wave Filter," *IEEE Transactions on Ultrasonics, Ferroelectrics, and Frequency Control*, vol. 49, no. 4, Apr. 2002, pp. 535-539.

[11] S.-H. Lee, J.-H. Kim, G.D. Mansfeld, K.H. Yoon, and J.-K. Lee, "Influence of Electrodes and Bragg Reflector on the Quality of Thin Film Bulk Acoustic Wave Resonators," *IEEE International Frequency Control Symposium and PDA Exhibition*, 2002, pp. 45-49.

[12] B.P. Otis and J.M. Rabaey, "A 300-μW 1.9-GHz CMOS Oscillator Utilizing Micromachined Resonators," *IEEE J. Solid-State Circuits*, vol. 38, no. 7, July 2003, pp. 1271-1274.

[13] T. Yokoyama, T. Nishihara, S. Taniguchi, M. Iwaki, Y. Satoh, M. Ueda, and T. Miyashita, "New Electrode Material for Low-loss and High-Q FBAR Filters," *Proc. IEEE 2004 Ultrasonics Symposium*, vol. 1, pp. 429-432.

[14] B. Ha, I. Song, Y. Park, D. Kim, W. Kim, K. Nam, and J.J. Pak, "Novel 1-chip FBAR Filter for Wireless Handsets," *Int. Conf. on Solid-State Sensors, Actuators, and Microsystems Dig. Tech. Papers*, 2005, vol. 2, pp. 2069-2073.

[15] H. Zhang, J. Kim, W. Pang, H. Yu, and E.S. Kim, "5GHz Low-phase-noise Oscillator Based on FBAR with Low TCF," *Int. Conf. on Solid-State Sensors, Actuators, and Microsystems Dig. Tech. Papers*, 2005, vol. 1, pp. 1100-1101.

[16] J.D. Larson III, P.D. Bradley, S. Wartenberg, and R.C. Ruby, "Modified Butterworth-Van Dyke Circuit for FBAR Resonators and Automated Measurement System," *Proc. IEEE 2000 Ultrasonics Symp.*, vol. 1, pp. 863-868.

[17] A.P.S. Khanna, E. Gane, and T. Chong, "A 2GHz Voltage Tunable FBAR Oscillator", *IEEE MTT-S Digest 2003*, vol. 2, pp. 717-720.

[18] Y.H. Chee, A.M. Niknejad, and J. Rabaey, "A Sub-100μW 1.9-GHz CMOS Oscillator Using FBAR Resonator, " *IEEE RFIC Symposium 2005 Dig. Papers*, pp. 123-126.

[19] J.J. Kim, H. Zhang, W. Pang, H. Yu, and E.S. Kim, "Low Phase Noise, FBAR-Based Voltage Controlled Oscillator without Varactor," *Int. Conf. on Solid-State Sensors, Actuators, and Microsystems*, 2005, vol. 1, pp. 1063-1066.

[20] T.A. Hansen, "Transistor Oscillatory Control Circuit", *US Patent 2,912,654*, November 10, 1959.

[21] C.H. Feistel and P.T. Gianos, "Butler Oscillator", *US Patent 3,996,530*, December 7, 1976.

[22] T.C. Lam, "Adjustable Crystal Oscillator with Separate Feedback Amplifier", *US Patent 3,319,186*, May 9, 1967.

[23] W.E. McKinzie III, "Drift-Equalized, Multi-Frequency Oscillator", *US Patent 4,573,025*, February 25, 1986.

[24] N.T. Tchamov and P. Jarske, "New High-Performance Voltage-Controlled LC-Oscillator", *IEEE MTT-S Digest 1996*, vol. 3, pp. 1511-1514.

[25] V. Stoyanov, I.S. Uzunov, and N.T. Tchamov, "Semi-symbolic analysis (SSA) for amplitude control design of series resonance low-voltage VCO", *IEE Electronics Letters*, vol. 36, no. 3, 6 Feb. 2003, pp. 264-266.

[26] P.R. Gray, P.J. Hurst, S.H. Lewis, and R.G. Meyer, *Analysis and Design of Analog Integrated Circuits*, 4th ed., John Wiley & Sons, 2001, pp. 183-186.

Appendix 1: Side-Applications of High-*Q* Oscillators

Oscillators based on high-*Q* resonators are interesting tools for educative investigations of the effects of tolerance variations and outside disturbances on oscillator operation. This chapter will discuss the use of Lissajous-figures in investigating oscillators and the effects that power supply disturbances have on oscillator performance. A simple testbench for evaluating these effects will also be proposed.

Lissajous-figures in oscillator investigation

Signals are most often plotted in time domain or frequency domain. This means that the y-axis of the plot denotes the magnitude of the signal, while the x-axis denotes either time or frequency. However, it is also possible to plot two signals against each other, so that all possible values of one signal correspond to points on the y-axis and the values of another signal correspond to points on the x-axis. These plots are called Lissajous-figures, an example of which is given in Figure 1.

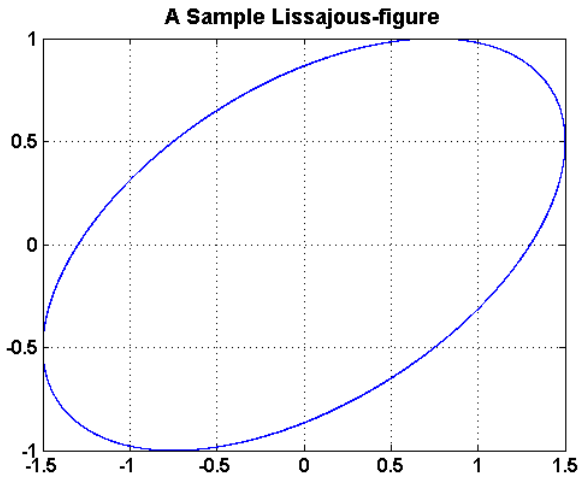

Figure 1. A sample Lissajous-figure.

Mathematically these figures are defined as follows:

$$x = A\sin(at + \varphi)$$

$$y = B\sin(bt)$$

In these equations, A and B stand for the magnitudes of the two different signals, a and b stand for the angular frequencies, and φ stands for the phase shift between the two signals. Depending on the ratio of the signal magnitudes, the ratio of the signal frequencies, and the phase shift, the Lissajous-figure can thus assume various shapes. In electrical measurements these figures can easily be produced by using an oscilloscope that can plot two channels against each other [1]. The resulting figures provide excellent education opportunities through challenges in deriving visually-based conclusions about oscillator performance.

One of the simplest applications of Lissajous-figures in oscillator investigations is to use the output signals of two theoretically identical oscillators as inputs signals to the oscilloscope. Theoretically the outputs of the oscillators should have the same amplitude and frequency, and the phase shift between the two should be zero. Therefore the Lissajous-figure should produce a simple line corresponding to the equation x = y.

However, as in all real-world implementations, these two basically identical oscillators will have output signals that differ from each other. This difference is seen in in amplitude and in frequency, and there will also be some phase shift between the two signals. The effects of these variations on the Lissajous-figure are shown separately in the following figures.

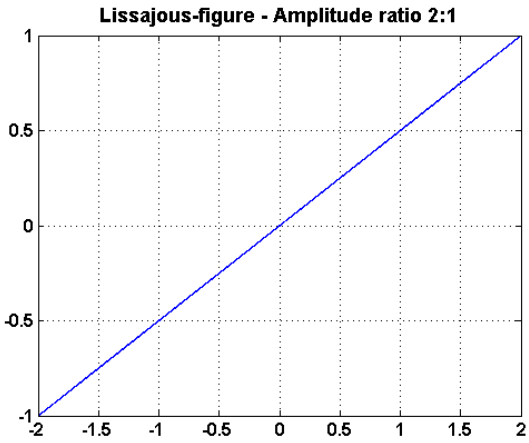

Figure 2. Lissajous-figure, amplitude ratio 2 : 1. Frequency and phase are equal.

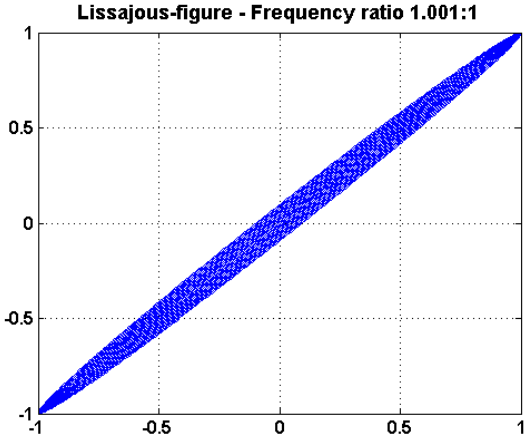

Figure 3. Lissajous-figure, frequency ratio 1.001 : 1. Amplitude and phase are equal, picture is for a few periods of the signal.

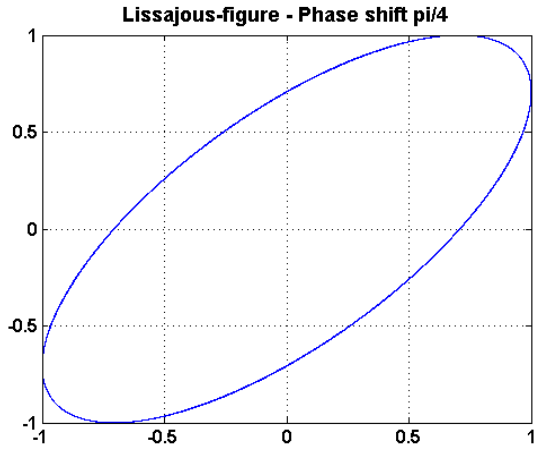

Figure 4. Lissajous-figure, phase shift of $\pi/4$ between the signals. Amplitude and frequency are equal.

The Lissajous-figure received from the measurement of two real oscillators will then be some combination of these figures, because there is variation in all of the parameters simultaneously. For example phase noise, which is a measure of frequency instability (causing small frequency differences between the two oscillators), will result in the figure being unstable and rotating. Figure 3 illustrates the figure for two signals differing in frequency. The figure shows the overlaid plots from a short period of time, since spanning a larger time period and overlaying the plots would fill the entire plot window. Instead of a line or an ellipsis, there is a spot on the screen that moves around. Larger frequency differences will cause plots such as the one in Figure 5.

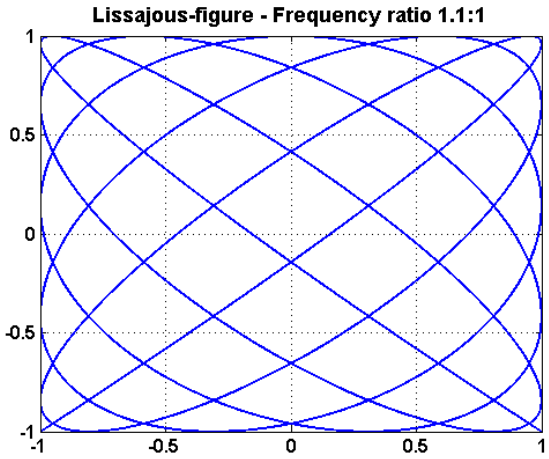

Figure 5. Lissajous-figure, frequency ratio 1.1 : 1. Amplitude and frequency are equal.

Power supply noise and oscillators

In the ideal case, the power supply used to provide current to electric circuits produces a clean signal, meaning a DC component and no AC components. However, this is never achieved to full extent even with complicated filtering techniques. Therefore the power supply voltage always contains a DC component and various AC components. The AC components can consist of wideband noise or for example of noise peaks on certain frequencies.

In addition to suffering from power supply noise, electronic circuits also create noise within themselves. Perhaps one of the most important types of noise in high-frequency circuits such as oscillators is the noise created in semiconductor components.

For example transistors exhibit various types of noise, with so-called flicker noise (also referred to as 1/f noise) being potentially very harmful for oscillator frequency stability. What makes this noise especially undesirable is that although it diminishes in its basic form as one moves to higher frequencies and is virtually non-existent at RF, it is upconverted to RF and superpositioned on the phase noise skirt of the carrier signal [2].

Similarly to semiconductor noise, power supply noise also has an effect on oscillators. Depending on the type and spectral content of the noise, the phase noise of the oscillator will be affected differently. Power supply noise is usually the external noise source causing the greatest deterioration in phase noise [3].

Proposed testbench for performance evaluation

In the following, I will propose a simple testbench for evaluating oscillator performance through Lissajous-figures and through the noise-affected spectral content of the output signal. The testbench must fulfill at least the following criteria:

- Possibility to use two identical oscillators
- Possibility to source the oscillators from the same power supply or from two different power supplies
- Possibility to insert noise to the power supply input or to the control voltage input of the oscillator
- Possibility to assess the effect of a voltage regulator

The block diagram of the solution arrived at for fulfilling these requirements is shown in Figure 6. A large amount of jumpers is included in order to make the PCB as versatile as possible for future experiments.

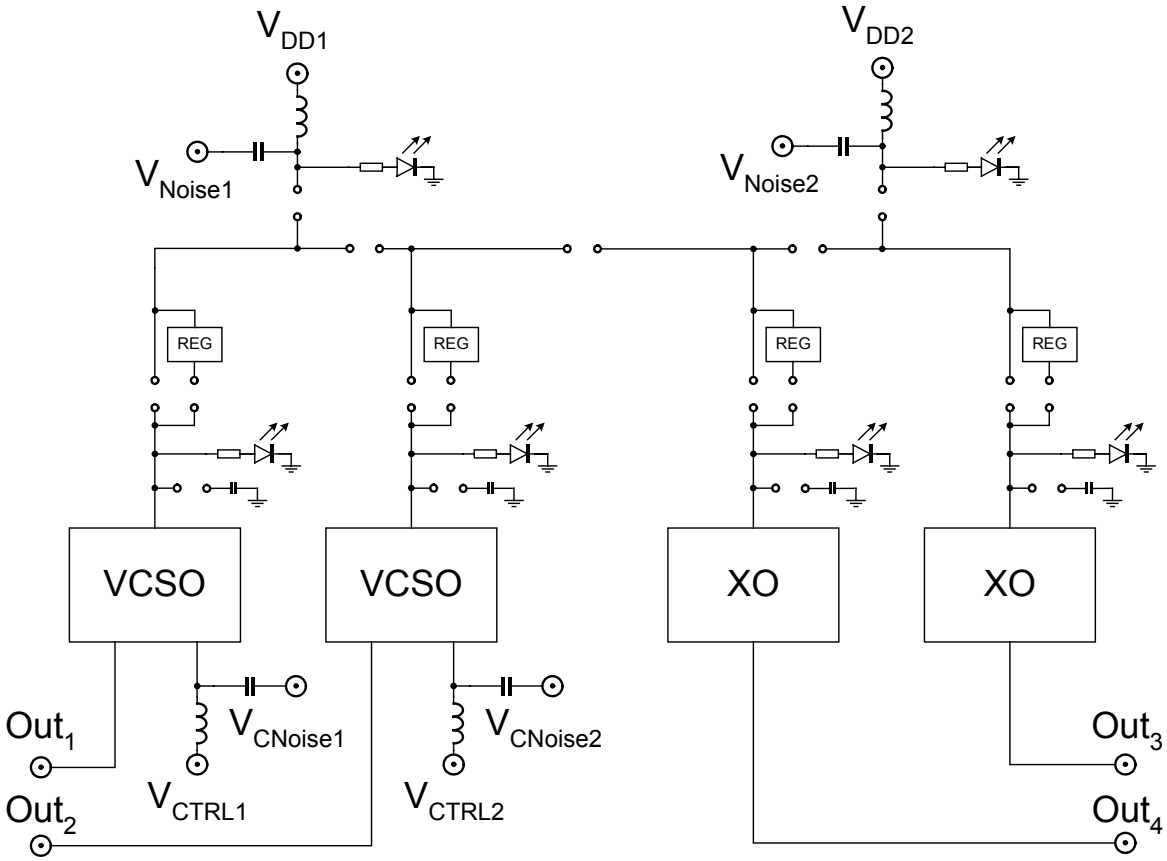

Figure 6. Block diagram of proposed testbench.

The testbench allows the use of four high-*Q* oscillators on the same board. In the proposed block diagram, two of the oscillators are SAW-based VCOs (VCSOs) and the two other are crystal oscillators (XO). It is possible to use a voltage regulator for each oscillator and also to use a DC-filtering capacitor on the power supply line. LEDs are attached at the main power supply input connectors and at the power supply inputs of each oscillator to inform the user of the presence of voltage.

Each pair of oscillators may share the same power supply or use separate power supplies. This allows one to use a noisy power supply voltage for one oscillator and to use a clean power supply voltage for the other one. Clear differences in the output signal spectrum should then be seen, and the two output signals can be compared simultaneously.

The easiest way to demonstrate Lissajous-figures is to feed one pair of oscillators from the same power supply. The oscillators should then operate under similar conditions and their comparison is fair. The Lissajous-figure can then be used to compare

the output amplitudes and frequencies of the oscillators, and they can be used to calculate the phase shift between the two output signals. Of course one can also use a VCSO and an XO to receive the Lissajous-figure, but in that case the resulting figure will be more complicated, especially if the two oscillators operate on clearly different frequencies.

Two of the basic ways to connect the proposed testbench for measurements are shown below in Figure 7 and Figure 8. In Figure 7, the two oscillators are fed from the same supply, and one of the basic measurements that can be done is to produce the Lissajous-figures with the oscilloscope. In Figure 8, one of the oscillators uses a noisy power supply while the other oscillator has a clean power supply. This setup can be used for example to compare the spectrum of the oscillator output signals with each other. One can also insert low-frequency noise through the control voltage input and see its upconversion to the RF spectrum of the output signal.

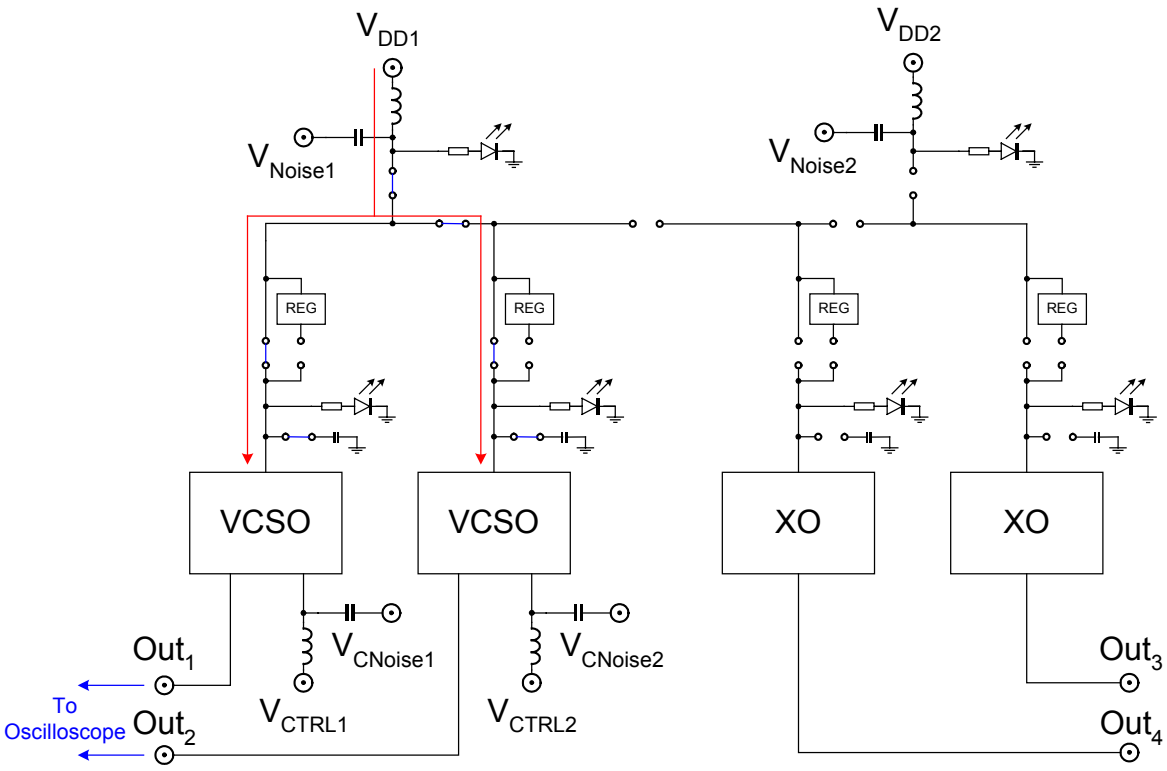

Figure 7. Two oscillators fed by the same supply.

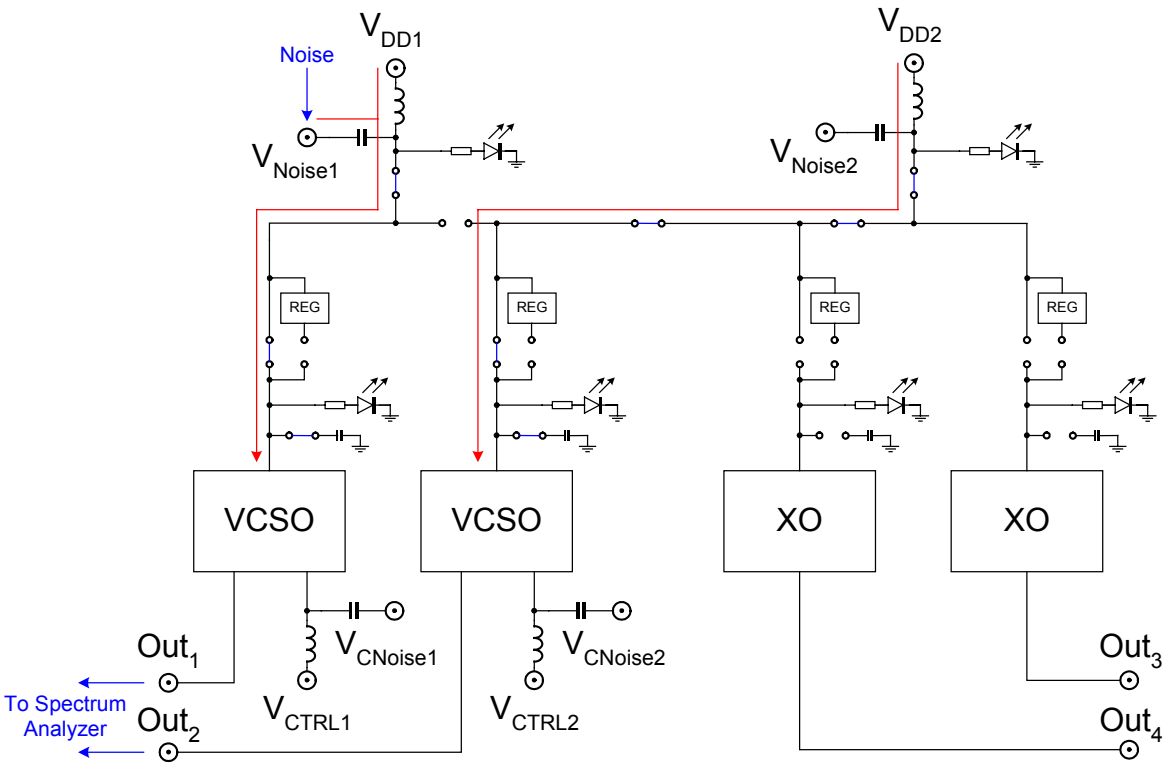

Figure 8. Two oscillators fed by separate supplies, one of them clean and the other one noisy.

References

[1] *User and Service Guide, HP 54600-Series Oscilloscopes*, June 1992, pp. 58-61.

[2] J.A. Babcock, B. Loftin, P. Madhani, X. Chen, A. Pinto, and D.K. Schroder, "Comparative Low Frequency Noise Analysis of Bipolar and MOS Transistors Using an Advanced Complementary BiCMOS Technology," *Proc. IEEE Custom Integrated Circuits Conference*, 2001, pp. 385-388.

[3] R. Fetche, C. Fetche, T. Fiez, and K. Mayaram, "Analysis of the Effects of Supply Noise Coupling on Phase Noise in Integrated LC CMOS Oscillators," *Proc. IEEE Radio and Wireless Conference*, 2000, pp. 199-202.

Appendix 2: Publication on the FBAR VCO

The following manuscript was submitted for review to the *IEEE Journal of Solid-State Circuits* on November 7, 2005. At the time of printing this thesis, no editorial decision with respect to publication had been made.

Kim B. Östman, Sami T. Sipilä, Ivan S. Uzunov, and Nikolay T. Tchamov

"Novel Monolithic VCO Architecture Using Series Above-IC FBAR and Parallel LC Resonance"

Appendix 3: Publication on an LC VCO

The following manuscript was submitted for review to the *IEEE Journal of Solid-State Circuits* on August 25, 2005. At the time of printing this thesis, no editorial decision with respect to publication had been made.

Sami T. Sipilä, Ivan S. Uzunov, Kim B. Östman, and Nikolay T. Tchamov

"Novel High-Performance VCO Architecture Based on the Simultaneous Use of Series and Parallel Resonance Tanks"
